Západočeská univerzita v Plzni

Fakulta aplikovaných věd

Smíšené metody v problémech nelineární elasticity velkých distorzí

Ing. Tomáš Svatoň

disertační práce
k získání akademického titulu *doktor*
v oboru *Aplikovaná matematika*

Školitel: Doc. Ing. Josef Daněk, Ph.D.
Katedra: Katedra matematiky

Plzeň 2012

University of West Bohemia

Faculty of Applied Sciences

Mixed methods in problems of finite elasticity with large distortions

Ing. Tomáš Svatoň

A thesis to obtain the academic degree of
Doctor of Philosophy
in the field *Applied mathematics*

Advisor: Doc. Ing. Josef Daněk, Ph.D.
Department of Mathematics

Plzeň 2012

Anotace

Analýza velkých elastických deformací materiálů s vlastnostmi podobných gumě je moderní disciplínou v mnoha odvětvích výzkumu, jako například v biomechanice aktivních polymerů či nematických elastomerů (funkční biomateriály a implantáty).

Co se týče biomechaniky problém spočívá v pokusu o sestavení matematicko-fyzikálních modelů pomocí nichž je možný popis fyziologického chování živých tkání od pokožky a svalu až ke tvrdým strukturám jako je chrupavka či kost. Biomechanická analýza a její validace skrze experimentální pokusy *in vivo* a *in vitro* může být pomocnou metodou neinvazivních lékařských diagnóz, plánování chirurgických zákroků či navrhování speciálních protéz.

V našem případě jsme se především zabývali vývojem matematického modelu kontrakce srdeční tkáně založeného na představě aktivních distorzí. Následovně byla provedena programová implementace s cílem provést sérii numerických výpočtů.

Ve druhém kroku bylo nezbytné vyřešit rozlišné numerické problémy, jako konvergence, efekt „locking“, regularita řešení či vhodné využití výpočetních zdrojů.

Předkládaná práce je zaměřena na analýzu porovnání různých numerických schémat aplikovaných na testovací příklad, aby jednotlivá obdržená řešení mohla být snadno konfrontována.

Konkrétně jsou formulovány tři numerické metody: kompatibilní, smíšená a de Veubeke–Hu–Washizu (dVHW) formulace.

Hlavním studovaným problémem v textu práce jsou nechtěné oscilace, které vznikají v oblasti nespojitosti distorze materiálu. Cílem zkoumání je ukázat, jak použitím dVHW metody najít řešení omezující tyto oscilace.

Pro vylepšení kvality řešení mohou být voleny dva hlavní směry: obměna numerického schématu nebo přizpůsobení formy výpočetní sítě. Na dvoudimenzionálním testovacím případě je ukázáno, že dVHW metoda může vykazovat lepší výsledky nežli původní smíšená metoda.

Problém optimalizace sítě za účelem lepší aproximace řešení lze analyzovat v jednodimenzionálním příkladě pomocí něhož je také určena numerická chyba řešení nabízených integračních schémat.

Klíčová slova: de Veubeke–Hu–Washizu, konečné prvky, smíšená metoda, nelineární elasticita, distorze, oscilace, biomechanika

Abstract

The analysis of rubber-like materials undergoing large elastic deformations is a key topic in field of active polymers, like ionic polymers, hydrogels and nematic elastomers, as well as in biomechanics, for soft tissues.

For biomechanics, the hot issue relays in the development of mathematical-physical models that are able to describe the behaviour of physiological processes involving highly deformable tissues, like the skin or the muscles, or hard tissue as cartilage and bones.

Such bio-mechanical models and their validation through experiments *in vivo* or *in vitro* can be helpful for better understanding physiological processes, for the planning of surgical interventions, or even for designing advanced prosthetic devices.

In our case, we focused on the development of a model that describes the contraction of cardiac tissue based on the notion of active distortions. Then, our model has been implemented in a computational code in order to asses its performance through a series of numerical experiments.

This second step brought us to face some tough problems, like convergence, locking effect, irregular solutions, together with a careful design of numerical test in order to optimize the computational resources.

The present work presents a comparative analysis of the performances of different numerical schemes applied to the solution of a reference benchmark problem.

All in all, there are proposed three numerical schemes, based on a compatible method, a mixed method, and the de Veubeke–Hu–Washizu (dVHW) one.

An important feature analyzed in the present thesis are the spurious oscillations of the solution which arise in the neighborhood of a jump of the distortion field. The goal of the research is to demonstrate how it is possible to find a solution without these oscillations using the dVHW method.

To improve the quality of the solution one may follows two main directions, one related to the numerical scheme, the other to the adaptation of the mesh. For one of our two-dimensional examples, it is demonstrated how, for a given mesh, the dVHW method yields better results than using the mixed formulation.

The optimization of the mesh as a strategy to improve the approximation of the solution, has been analyzed in a one-dimensional example, which gives insight on the origin of some computational error in the proposed integration schemes.

Keywords: de Veubeke–Hu–Washizu, finite elements, mixed method, nonlinear elasticity, distortion, oscillation, biomechanics

Sommario

L'analisi dei materiali con proprietà simili alle gomme, ossia, suscettibili di grandi deformazioni elastiche, ha acquistato sempre più rilevanza nel settore della biomeccanica o dei polimeri attivi, come i polimeri ionici, gli idrogel o gli elastomeri nematici.

Per quanto riguarda la biomeccanica, l'importanza risiede nel tentativo di mettere a punto modelli fisico-matematici in grado di descrivere il comportamento dei processi fisiologici che coinvolgono i tessuti soffici, come la pelle o i muscoli, ovvero, ai tessuti duri, come cartilagini e ossa; la modellazione biomeccanica e la sua validazione attraverso prove sperimentali *in vivo* od *in vitro* può essere di ausilio alle indagini mediche non invasive o alla pianificazione degli interventi chirurgici, nonché alla progettazione di protesi avanzate.

Nel nostro caso, ci siamo innanzitutto occupati dello sviluppo di un modello fisico-matematico della contrazione del tessuto cardiaco basato sulla nozione di distorsioni attive; in seguito, il modello è stato implementato in un codice computazionale con l'obbiettivo di avviare una campagna di esperimenti numerici.

Questo secondo passo ci ha portato ad affrontare diversi problemi, come la convergenza, l'effetto "locking", la regolarità della soluzione, l'uso accurato delle risorse di calcolo.

Il presente lavoro consiste nell'analisi comparativa di vari schemi numerici applicati ad uno stesso problema campione, così da confrontare i vari risultati ottenuti.

In totale sono proposti tre schemi numerici: il metodo compatibile, quello misto e il cosiddetto metodo di de Veubeke–Hu–Washizu (dVHW).

Il problema principale studiato nella presente tesi sono le oscillazioni spurie della soluzione che hanno origine nelle zone di discontinuità del campo delle distorsioni. Lo scopo della ricerca è dimostrare come sia possibile, usando il metodo dVHW, trovare una soluzione limitando queste oscillazioni.

Per migliorare la qualità delle soluzioni si possono seguire due diverse strategie: il cambiamento dello schema numerico, oppure un adattamento del reticolo. Su un esempio numerico bidimensionale è stato dimostrato come il metodo dVHW, a parità di reticolo, fornisca risultati migliori rispetto a quelli ottenuti dalla formulazione mista.

Il problema della ottimizzazione del reticolo ai fini della migliore approssimazione della soluzione si può analizzare nell'esempio monodimensionale da cui è stato ricavato l'errore computazionale ottenuto da schemi di integrazione proposti.

Parole chiavi: de Veubeke–Hu–Washizu, elementi finiti, metodo misto, elasticità nonlineare, distorsione, oscillazione, biomeccanica

Résumé

L'analyse des matériels avec des propriétés similaires à celles du caoutchouc, c'est-à-dire susceptibles de grandes déformations élastiques, a acquis une grande importance dans le secteur de la biomécanique ou des polymères actifs comme les polymères ioniques, les hydrogels ou les élastomères nématiques.

En ce qui concerne la biomécanique, l'importance réside dans les tentatives de mettre au point des modèles physico-mathématiques en mesure de décrire le comportement des processus physiologiques qui impliquent des tissus conjonctifs, comme la peau ou les muscles ou bien les tissus durs, tel que les cartilages et les os ; la modulation biomécanique et sa validation à travers l'épreuve expérimentale *in vivo* ou *in vitro* peut être utile pour des enquêtes médicales non invasives ou pour la planification des interventions chirurgicales, mais aussi pour le projet de prothèses avancées.

Dans notre cas, nous nous sommes avant tout occupés du développement d'un modèle physico-mathématique de la contraction du tissu cardiaque fondé sur la notion de distorsions actives ; ensuite, le modèle a été implémenté avec un code de calcul ayant pour objectif de lancer une série d'expériences numériques.

Cette seconde étape nous a conduits à affronter des problèmes divers, comme la convergence, l'effet « locking », la régularité de la solution, l'emploi adéquat des ressources du calcul.

Le présent travail consiste en l'analyse comparative de schémas numériques variés appliqués sur un même étalon problème pour comparer les différents résultats obtenus.

Au total nous proposons trois schémas numériques : la méthode compatible, le mixte et le dénommé de Veubeke–Hu–Washizu méthod (dVHW).

Le problème principal étudié dans notre thèse est les oscillations apocryphes de la solution qui ont leur origine dans la zone de la discontinuité du champ des distorsions. Le but de la recherche est de montrer comment il est possible, en utilisant la méthode dVHW, de trouver une solution en limitant ces oscillations.

Afin d'améliorer la qualité de la solution on peut suivre deux stratégies différentes : le changement du schéma numérique, ou bien une adaptation du maillage. Dans un exemple numérique bidimensionnel nous avons montré comment la méthode dVHW, à égalité de maillage, fournit de meilleurs résultats par rapport à ceux obtenus par la formulation mixte.

Le problème de l'optimisation du maillage dans le but d'améliorer l'approximation de la solution peut s'analyser dans l'exemple unidimensionnel duquel a été déterminé l'erreur de calcul obtenu des schémas d'intégration proposés.

Mots-clés : de Veubeke–Hu–Washizu, éléments finis, méthode mixte, élasticité non lineaire, distorsion, oscillation, biomécanique

Declaration

I hereby declare that this doctoral thesis is my own work with the exclusion of the cited Bibliography sources.

Tomáš Svatoň

Acknowledgement

This thesis is based on the work that I began in Rome during my first nine month stay at the "Sapienza" University of Rome and completed later to its current form. During my doctoral study in Pilsen I had two opportunities to stay in Rome. For these possibilities I would like to express my gratitude to prof. Paola Nardinocchi and prof. Antonio Carcaterra. I would like to heartfully thank to doc. Josef Daněk for his great patience during his leading of my work and the good advice he always gave me. I remember as a very special occasion the possibility to speak about the topic of my thesis at the Czech Academy of Sciences in Prague which gave me prof. Petr Přikryl. I would also like to thank my family and friends who always trusted me. Their warm support was a real source of energy for me and helped me to conclude my work.

Last I gratefully acknowledge the ITN Marie Curie project GA-214909 "MID-FREQUENCY – CAE Methodologies for Mid-Frequency Analysis in Vibration and Acoustics".

Tomáš Svatoň

Contents

List of Figures

List of Figures

List of Tables

List of Tables

Glossary

∇ Gradient on the reference configuration. 8

$\otimes$ Dyadic product. 4

$\cdot$ Scalar product. 4

$\oplus$ Set addition. 4

$\times$ Cross (vector) product. 4

$\mathbf{a}$ Vector. 54

$\dot{\mathbf{a}}$ Material time derivative of the spatial vector field; $\dot{\mathbf{A}}$ material time derivative of the spatial tensor field. 8

$\mathbf{a}'$ Spatial time derivative of the spatial vector field. 8

$\|\mathbf{a}\|$ Length of the vector $\mathbf{a}$. 4

$\mathbf{A}^{\mathbf{T}}$ Transposed tensor of second order. 54

$\mathbf{A}^{\star}$ Cofactor of $\mathbf{A}$. 6

$\mathbf{A}^{-\mathbf{T}}$ Transposed and inverse tensor of $\mathbf{A}$; $\mathbf{A}^{-\mathrm{T}} = (\mathbf{A}^{\mathrm{T}})^{-1} = (\mathbf{A}^{-1})^{\mathrm{T}}$. 6

α Spatial scalar field function; α_m material scalar field function. 7

$\mathbf{B}$ Left Cauchy–Green deformation tensor. 7

$\mathscr{B}$ Reference body manifold; $\mathscr{B}_t$ actual body manifold. 4

Glossary

$\partial\mathscr{B}$ Boundary of reference body manifold; $\partial\mathscr{B}_t$ in the actual configuration; $\partial\mathscr{B}_k$ and $\partial\mathscr{B}_d$ boundary with assigned kinematic and dynamic boundary conditions. 4

$\mathbf{c}$ External (contact) force on actual configuration; $\bar{\mathbf{c}}$ on the reference one. 10

$\mathbf{C}$ Right Cauchy–Green deformation tensor; $\mathbf{C}_o$ its distorting form; $\mathbf{C}_e$ its elastic form; $\bar{\mathbf{C}}_e$ isochoric part of $\mathbf{C}_e$. 7

$C^0(\bar{\mathscr{B}})$ Space of all continuous functions on $\mathscr{B}$. 23

$\mathbf{d}$ Internal (bulk, distance) force; $\bar{\mathbf{d}}$ on the reference one. 10

$\mathbf{D}$ Stretching tensor. 8

d Space dimension. 23

da Area element in the actual configuration; dA its representation in the reference configuration. 6

dv Volume element in the actual configuration; dV its representation in the reference configuration. 6

dx Line element in the actual configuration; dX its representation in the reference configuration. 6

δl Local change in length; δa local change in area; δv local change in volume; $\delta\Pi$ variation of the potential energy of the system. 6

det Determinant of square matrix. 5

dev Deviatoric part of symmetric tensor. 14

div Divergence on the actual configuration; Div on the reference configuration. 54

Dsc Discontinuous element; Dsc_1 and Dsc_2 first and second order Lagrange element. 23

$\mathbf{E}$ Green–Lagrange deformation tensor. 7

ϵ Error of numerical solution. 48

$\mathscr{E}$ Euclidean space. 4

$\mathbf{F}$ Deformation gradient with components F_{ij}; $\tilde{\mathbf{F}}$ its variation, test function field; $\mathbf{F}_o$ distortion tensor with F_{oij} components; $\mathbf{F}_e$ and $\bar{\mathbf{F}}_e$ elastic deformation tensor and its isochoric part. 5

grad Gradient on the actual configuration. 8

$H^k(\mathscr{B})$ Inner product space. 20

I I_i the i-th principle invariant; I_{ei} invariant in terms of elastic deformation. 13

J Jacobian of deformation gradient $\mathbf{F}$; J_o Jacobian of $\mathbf{F}_o$; J_e Jacobian of $\mathbf{F}_e$. 5

K Element of triangulation. 21

κ Bulk modulus. 17

Lag Lagrange element; Lag_1 and Lag_2 first and second order Lagrange element. 23

$L^2(\mathscr{B})$ Space of real valued Lebesgue measurbale functions. 20

$\mathbb{L}\mathtt{in}$ Space of all linear tensors; $\mathbb{L}\mathtt{in}^+$ involve tensors with positive determinant. 4

λ Stretch caused by deformation $\boldsymbol{\chi}$; λ_o stretch caused by $\mathbf{F}_o$; stretch caused by $\mathbf{F}_e$. 6

$\mathbf{m}$ Oriented normal to $\mathscr{B}$. 6

M Space of all "integrable" functions; M_h finite dimensional subspace of M. 21

μ Shear modulus. 15

$\mathbf{n}$ Oriented normal to $\mathscr{B}_t$. 6

Glossary

$\mathbb{O}\mathtt{rt}$ Space of orthogonal tensors. 5

p Internal (hydrostatic) pressure; $\tilde{p}$ its variation, test function field. 14

P Space of a real valued functions over K – ansatz-functions. 22

$\mathscr{P}$ Body part in the reference configuration; $\mathscr{P}_t$ in the actual configuration. 11

Π Virtual power; Π^{est} and Π^{int} external and internal virtual power. 10

ψ Strain (stored, elastic potential) energy; ψ_o related to the distorted stance; ψ_{iso} and ψ_{vol} isochoric and volumetric part of ψ. 12

$\mathbf{Q}$ Orthogonal tensor in $\mathbb{O}\mathtt{rt}$. 5

$\mathbb{R}$ Set of real numbers. 4

$\mathbf{S}$ First Piola–Kirchhoff (reference) stress with components S_{ij}; $\tilde{\mathbf{S}}$ its variation, test function field; $\mathbf{S}_{iso}$ and $\mathbf{S}_{vol}$ isochoric and volumetric parts of the stress $\mathbf{S}$. 11

$\mathbf{S}_C$ Cosserat stress tensor associated to $\mathbf{C}$; $\mathbf{S}_E$ connected with $\mathbf{E}$. 13

$\mathbf{S}_o$ Energetic stress tensor related to the distorted configuration; $\mathbf{S}_e$ energetic stress in current configuration. 15

$\mathbb{S}\mathtt{kw}$ Space of all skew tensors; skw $\mathbf{A}$ mapping of tensor $\mathbf{A}$ to space $\mathbb{S}\mathtt{kw}$. 4

sph Spherical part of symmetric tensor. 14

$\mathbb{S}\mathtt{ym}$ Space of all symmetric tensors; sym $\mathbf{A}$ mapping of tensor $\mathbf{A}$ to space $\mathbb{S}\mathtt{ym}$. 4

Σ Set of basis functions defined over the triangulation T_h. 22

$\mathbf{T}$ Cauchy (actual, visible) stress; $\mathbf{T}_s$ spherical reactive stress; $\mathbf{T}_a$ active stress. 10

$\mathscr{T}$ Time line. 4

tr Trace of the tensor. 14

T_h Triangulation of a domain $\mathscr{B}$. 21

$\mathbf{u}$ Displacement; $\tilde{\mathbf{u}}$ its variation, test function field; $\bar{\mathbf{u}}$ assigned displecement as boundary condition on $\partial\mathscr{B}$. 5

$\|u\|_{L^2(\mathscr{B})}$ Norm of $u \in L^2(\mathscr{B})$. 20

$\|u\|_{H^k(\mathscr{B})}$ Norm in $H^k(\mathscr{B})$. 20

$(u, v)_{L^2(\mathscr{B})}$ Scalar product of u and v in $L^2(\mathscr{B})$. 20

$\mathbf{v}$ Spatial representation of the velocity field $\dot{\boldsymbol{\chi}} = \dot{\mathbf{u}} = \mathbf{v}_m$; It may denote also a virtual velocity field $\mathbf{v}$ on the actual configuration (then $\bar{\mathbf{v}}$ on the reference configuration), that is distinguished easily from the velocity field by the context. 8

V Space of all "integrable" functions until their first derivative; V_h finite dimentsional subspace of V. 21

$V\mathscr{E}$ Vector space associated to Euclidean space $\mathscr{E}$. 4

$\mathbf{w}$ Spatial vector field function; $\mathbf{w}_m$ material vector field function. 7

$\mathbf{W}$ Spin tensor. 8

W_h Finite dimensional subspace of M with no continuity requirements accross interelement boundaries. 23

$\boldsymbol{\chi}$ Motion – the spatial placement; $\tilde{\boldsymbol{\chi}}$ its variation. 5

x Point in the actual configuration; X point in the reference one. 5

Acronyms

BC boundary condition. 24

dof degrees of freedom. 32

dVHW de Veubeke–Hu–Washizu. 26

elems elements. 32

FE Finite Element. 3

PDE partial differential equation. 55

UV Ultra violet. 1

Chapter 1

Problem introduction

Modelling based on the theory of finite elasticity with large distortions is applied in various fields of mechanics. A first illustration could be given by the problem of description of the behaviour of soft living tissues, namely the cardiac muscle physiology. The result of such a research is the acquisition of non invasive techniques to study the human heart. At the present time this issue is a big challenge containing several open practical and theoretical questions, see (Nardinocchi et al., 2010) for further details. The second popular application of the non linear elasticity theory with large distortions can be found in the nematic elastomers mechanics, see (DeSimone and Teresi, 2009).

The modelling of soft tissues can be tackled in two main directions which are the active stress or the active strain. The differences between these two approaches are slightly sketched in chapter 2 with proper references to the contemporary literature. In this work for its mathematical robustness the active strain approach is chosen as the tool to perform the active soft tissues analysis. Note that the existence of works based on the active stress description (Rohan and Cimrman, 1999, 2002) was taken in account and the priority instruments therein leaved as an option of a possible later research direction.

Every substance supposed to be actively distorted is characterized by a large spontaneous deformation. In the cardiac tissue this is caused by the presence of free Ca^{2+} and in the nematic elastomers this mechanical behaviour can be activated by Ultra violet (UV) light, electric field or thermally. The studies of electromechanical properties of cardiac tissues in (Cherubini et al., 2008) are fo-

cused on the propagation of the activating signal as a wave in the living medium. In general such a wave or activated zone is characterized by a front with a very steep gradient or even discontinuity on the margins of the zone with exciting quantity. The solution of this kind of problem relative to the mechanical description can evince the oscillations near the front of the distorted part of the body. In the work this spurious phenomena in the solution is analysed to understand and consequently try to cancel it.

1.1 Objectives of the thesis

The electromechanical coupling is usually described as the convection diffusion problem. When its stationary form is considered then its mechanical part yields oscillations of the resulting stress appearing in the distortion discontinuity case. Hence the problem of the finite elasticity with large deformations and distortions is stabled and the non linear elliptic boundary value problem with discontinuity coefficients is to be solved. In this thesis nor the issue of existence and uniqueness, neither the convergence to the true solution of the problem is analysed, but are simply assumed to be fulfilled. For further informations about this topic a reader can be induced to see (Hartmann and Neff, 2006; Ženíšek, 1990).

The aim of this work is to improve the solution damping the oscillations as far as the de Veubeke–Hu–Washizu method is concerned. When the mixed method is applied then this effect can be observed, see (Wriggers, 2008). Thus two points of view are chosen to be taken into account, the form of the mesh and the used numerical scheme. There is also another factor to be taken into account, such as the type of used elements and the physical parameters of the model that are considered in order to obtain the best performance of the methods on the chosen benchmark. The analysis revealed that both factors, the mesh quality and the chosen method contributed to an improvement of the quality of the solution. Every model is implemented in the compatible, mixed and de Veubeke–Hu–Washizu formulation, see e.g. (Bathe, 1996; Hughes, 1987; Wriggers, 2008). The basic characteristics of meshes are selected according to its fineness and the ability to follow the critical zones as it is sketched in figure 2.1.

Both methods are used on the same mesh and it is possible to see a difference between the solutions obtained. Then the different meshes for each proposed

method are chosen simultaneously and the quality of solution compared. The plots with the solution are a good tool to get a first idea about how the solution behaves according to the used method and the mesh. Anyway this some kind of intuitive approach, as yields a good frame about used tools, is not sufficient.

The numerical benchmarks have to be prepared so that more exact tools are able to capture the differences on the used methods and meshes. Thus the three-, two- and one-dimensional examples are stabled to obtain an exact solution of the simplified three dimensional problems. To be able to relate these results of fewer dimensional benchmarks it is important to maintain in some way the consistency of the problem. Thus the geometry and the prescribed governing quantities are to be maintained.

For the implementation of the model we used the commercial Finite Element (FE) software *COMSOL Multiphysics*^{TM} *3.5a*, see (COM, 2008). The possibility to get the proper implementation through the other especially open source computational environment like SfePy, FEAPpv, or FreeFEM++ for instance, see (Cimrman and contributors, 2011; Hecht, 2011; Zienkiewicz et al., 2009), had also been taken into account, but was postponed due to the several complications encountered already during the implementation in COMSOL. It should be noted that for a special demands on the mesh the external generator GMSH is used, see (Geuzaine and Remacle, 2010). The way how proper numerical methods are implemented and mesh is imported can be found in Appendix B.

The work on this subject consists in several open questions and their summary can be found in the conclusion in chapter 5, where we also mention the other possible research directions.

Chapter 2

Continuum mechanics

In this chapter the basic relations used in continuum mechanics will be introduced so that it will be possible to capture the description of large deformations and distortions. In both sections 2.1 and 2.2, at first the concepts of conventional strain and stress measure will be introduced and then a generalization of the case with distortions will follow. The basic informations about kinematics are taken from the sources: (DiCarlo and Quiligotti, 2002; Gurtin, 1981; Podio-Guidugli, 2000).

2.1 Kinematics

Let $\mathscr{T}$ be the *time line* identified with the real line $\mathbb{R}$ and let $\mathscr{E}$ be the three-dimensional *Euclidean space* and $V\mathscr{E}$ the associated vector space, which is endowed with the inner *scalar product* $\mathbf{a}\cdot\mathbf{b}$ and the *cross product* $\mathbf{a}\times\mathbf{b}\in V\mathscr{E}$ of two elements $\mathbf{a},\mathbf{b}\in V\mathscr{E}$. Thanks to the first inner product the *length* of a vector $\mathbf{a}$ can be defined as $\|\mathbf{a}\| = (\mathbf{a}\cdot\mathbf{a})^{\frac{1}{2}}$. This Euclidean space will be equipped with the *Cartesian frame* $\{o,\mathbf{c}_1,\mathbf{c}_2,\mathbf{c}_3\}$, where $o\in\mathscr{E}$ is the *origin*, $\mathbf{c}_i\in V\mathscr{E}$, $i=1,2,3$ is an orthonormal *basis*. With $\mathscr{B}$ is introduced the smooth body manifold (identified with its reference shape) with boundary $\partial\mathscr{B}$.

The set of all linear second order tensors which map $V\mathscr{E}$ into itself will be de-

noted as

$$\mathbb{L}\mathtt{in} := \{\mathbf{A} : V\mathscr{E} \xrightarrow{\text{lin.}} V\mathscr{E}\} \quad \text{and} \quad \mathbb{L}\mathtt{in} = V\mathscr{E} \otimes V\mathscr{E} = \mathbb{S}\mathtt{ym} \oplus \mathbb{S}\mathtt{kw}\,, \tag{2.1}$$

where $\mathbb{S}\mathtt{ym}$ and $\mathbb{S}\mathtt{kw}$ are the subsets of all *symmetric* and *skew* tensors whose elements have the following properties

$$2\mathrm{sym}\,\mathbf{A} = \mathbf{A} + \mathbf{A}^{\mathrm{T}} \in \mathbb{S}\mathtt{ym}\,, \quad 2\mathrm{skw}\,\mathbf{A} = \mathbf{A} - \mathbf{A}^{\mathrm{T}} \in \mathbb{S}\mathtt{kw}\,. \tag{2.2}$$

Let $\mathbf{A}\cdot\mathbf{B}$ be a scalar product of two tensors in $\mathbb{L}\mathtt{in}$ and $\mathbf{a}\otimes\mathbf{b} \in \mathbb{L}\mathtt{in}$ be a dyadic product of two vectors from $V\mathscr{E}$. An important group is a set of all gradients of all rotations in $\mathbb{L}\mathtt{in}$ called *orthogonal group* denoted as

$$\mathbb{O}\mathtt{rt} := \{\mathbf{Q} \in \mathbb{L}\mathtt{in} : \ \mathbf{Q}^{\mathrm{T}}\mathbf{Q} = \mathbf{Q}\mathbf{Q}^{\mathrm{T}} = \mathbf{I}\}\,. \tag{2.3}$$

2.1.1 Motion

The spatial placement, the *motion*, is understood as any smooth embedding

$$\begin{aligned} \boldsymbol{\chi} : \mathscr{B} \times \mathscr{T} &\to \mathscr{E} \\ (X, t) &\mapsto x = \boldsymbol{\chi}(X, t) = X + \mathbf{u}(X, t) \end{aligned} \tag{2.4}$$

of the body into the euclidean space $\mathscr{E}$ associating to any material point $X \in \mathscr{B}$ its position in the space $x = \boldsymbol{\chi}(X, t) \in \mathscr{E}$. The vector valued field $\mathbf{u} = x - X$ represents the *displacement* of the material point X. The set $\mathscr{B}_t = \boldsymbol{\chi}(\mathscr{B}, t)$ represents the *actual configuration* of a body $\mathscr{B}$ at a time t, within $\partial\mathscr{B}_t$ as its boundary.

It should be noted that every one-to-one, smooth and locally orientation-preserving mapping (2.4) is called *deformation* of the body and satisfies

$$\det \nabla\boldsymbol{\chi}(X, t) > 0\,, \ X \in \mathscr{B}\,. \tag{2.5}$$

The *deformation gradient* $\mathbf{F} \in \mathbb{L}\mathtt{in}$ and the *Jacobi determinant* J of $\mathbf{F}$ will be defined as

$$\mathbf{F} := \nabla\boldsymbol{\chi} = \mathbf{I} + \nabla\mathbf{u}\,, \quad J := \det\mathbf{F}\,. \tag{2.6}$$

As far as a definition of the deformation (2.5) is concerned the space of all ten-

sors with a positive determinant will be denoted $\mathbb{L}\mathtt{in}^{+}$. Let a hierarchy be of infinitesimally small one-, two- and three-dimensional parallepipedal cells, built out of the vectors $\mathbf{a}, \mathbf{b}, \mathbf{c} \in V\mathscr{E}$ attached to a place $X \in \mathscr{B}$:

1. an oriented line element $(\mathbf{a})$ represented by a vector $\mathbf{a}$
2. an oriented surface element $(\mathbf{a}, \mathbf{b})$ represented by a vector product $\mathbf{a} \times \mathbf{b}$
3. an oriented volume element $(\mathbf{a}, \mathbf{b}, \mathbf{c})$ represented by the oriented volume $\mathbf{a} \times \mathbf{b} \cdot \mathbf{c}$.

Their images after the action of $\boldsymbol{\chi}$ attached to the actual position $x = \boldsymbol{\chi}(X, t) \in \mathscr{B}_t$ in the space are

1. $\mathbf{F}(X, t)\mathbf{a}$
2. $\mathbf{F}^{\star}(X, t)(\mathbf{a} \times \mathbf{b}) = (\mathbf{F}(X, t)\mathbf{a}) \times (\mathbf{F}(X, t)\mathbf{b})$
3. $J(X, t)(\mathbf{a} \times \mathbf{b} \cdot \mathbf{c}) = (\mathbf{F}(X, t)\mathbf{a}) \times (\mathbf{F}(X, t)\mathbf{b}) \cdot (\mathbf{F}(X, t)\mathbf{c})$

Here $\mathbf{A}^{\star} = (\det \mathbf{A})\mathbf{A}^{-\mathrm{T}}$ is the *cofactor* of $\mathbf{A} \in \mathbb{L}\mathtt{in}^{+}$. It is worth noting that from 2 can be deduced a rule which relates the normal $\mathbf{m}$ oriented to $\partial\mathscr{B}$ to its image $\mathbf{n}$ oriented to $\partial\mathscr{B}_t$ as follows

$$\mathbf{n} = \frac{\mathbf{F}^{\star}\mathbf{m}}{\|\mathbf{F}^{\star}\mathbf{m}\|} \tag{2.7}$$

Therefore the line, area and volume elements associated to the reference and actual configuration are mapped as follows

$$dx = \mathbf{F}\, dX\,, \quad da = \|\mathbf{F}^{\star}\mathbf{m}\| dA\,, \quad dv = J dV\,. \tag{2.8}$$

Let a pair $(X, \mathbf{e})$ denotes a *material fibre* through a point X in direction $\mathbf{e}$ and its image be $(\boldsymbol{\chi}(X, t), \mathbf{F}(X, t)\mathbf{e})$, then the *local change in length* $\delta l(\mathbf{e})$ at X of a fibre $(X, \mathbf{e})$ is

$$\delta l(\mathbf{e}) = \|\mathbf{F}\mathbf{e}\| - 1\,. \tag{2.9}$$

Thus the *strech* λ of the fibre $(X, \mathbf{e})$ can be defined as follows

$$\lambda(\mathbf{e}) := 1 + \delta l(\mathbf{e}) = \|\mathbf{F}\mathbf{e}\|\,. \tag{2.10}$$

In the same way the changes in area and volume are

$$\delta a(\mathbf{m}) = \|\mathbf{F}^{\star}\mathbf{m}\| - 1\,, \quad \delta v = \det \mathbf{F} - 1\,. \tag{2.11}$$

2.1.2 Strain measures

For the local analysis of deformation the mostly used strain measures will be considered together with their physical meanings. About the definition of the stretch (2.10) it is possible to write

$$\lambda(\mathbf{e}) = (\mathbf{C}\cdot\mathbf{e}\otimes\mathbf{e})^{\frac{1}{2}}\,, \quad \text{where} \quad \mathbf{C} = \mathbf{F}^{\mathrm{T}}\mathbf{F} \in \mathbb{S}\mathtt{ym}\,, \tag{2.12}$$

being the *right Cauchy–Green deformation tensor*. Another strain measure used in continuum mechanics is defined as

$$\mathbf{B} = \mathbf{F}\mathbf{F}^{\mathrm{T}} \in \mathbb{S}\mathtt{ym} \tag{2.13}$$

and is called the *left Cauchy–Green deformation tensor*. Both these strains are exact so far as they measure the length deformation of the fibre with no approximation. When the change-length approximation is considered as the first degree polynom of the Taylor series it is possible to write

$$\delta l(\mathbf{e}) = ((\mathbf{I}+2\mathbf{E})\cdot\mathbf{e}\otimes\mathbf{e})^{\frac{1}{2}} \approx \mathbf{E}\cdot\mathbf{e}\otimes\mathbf{e}\,, \quad \mathbf{E} = \frac{1}{2}(\mathbf{C}-\mathbf{I})\,. \tag{2.14}$$

This deformation measure is called the *Green–Lagrange strain measure*. It should be noted that no deformation implies $\mathbf{C} = \mathbf{B} = \mathbf{I}$ and $\mathbf{E} = \mathbf{0}$.

2.1.3 Spatial and material fields

This subsection is based on the theory discussed in (Gurtin, 1981). When the balance principles are settled, the relations between the quantities in the reference and the actual configuration are needed. In these terms every *material field function* is associated with the domain $\mathscr{B}\times\mathscr{T}$ and the *spatial field function* with

$\mathscr{B}_t \times \mathscr{T}$. Let be considered a spatial scalar α and a vector field $\mathbf{w}$ respectively:

$$\begin{aligned} \alpha &: \mathscr{B}_t \times \mathscr{T} \to \mathbb{R}\,, \quad (X,t) \mapsto \alpha(X,t)\,, \\ \mathbf{w} &: \mathscr{B}_t \times \mathscr{T} \to V\mathscr{E}\,, \quad (X,t) \mapsto \mathbf{w}(X,t)\,. \end{aligned} \tag{2.15}$$

That is the material description of the spatial field. Then the corresponding spatial description of a material field will be defined as the following composition of maps

$$\alpha_m = \alpha \circ \boldsymbol{\chi}\,, \quad \mathbf{w}_m = \mathbf{w} \circ \boldsymbol{\chi}\,. \tag{2.16}$$

Then the material gradient "∇" of the material field is related to the spatial gradient "grad" of the spatial field as follows

$$\begin{aligned} \nabla\alpha_m = \mathbf{F}^{\mathrm{T}}(\operatorname{grad}\alpha)_m \Leftrightarrow\ (\operatorname{grad}\alpha)_m = \mathbf{F}^{-\mathrm{T}}\nabla\alpha_m\,, \\ \nabla\mathbf{w}_m = (\operatorname{grad}\mathbf{w})_m\mathbf{F} \Leftrightarrow\ (\operatorname{grad}\mathbf{w})_m = \nabla\mathbf{w}_m\mathbf{F}^{-1}\,. \end{aligned} \tag{2.17}$$

Distinguishing with a dot the material time derivative of the spatial fields, i.e. $\dot{\mathbf{a}}$, and with a prime the spatial time derivative of the spatial field, i.e. $\mathbf{a}'$, it holds

$$\dot{\alpha} = \operatorname{grad}\alpha \cdot \mathbf{v} + \alpha'\,, \quad \dot{\mathbf{w}} = \operatorname{grad}\mathbf{w}\mathbf{v} + \mathbf{w}'\,, \tag{2.18}$$

where $\mathbf{v}$ is the spatial representation of the velocity field $\dot{\boldsymbol{\chi}} = \dot{\mathbf{u}} = \mathbf{v}_m$. Therefore as far as the material time rate of change of deformation of a continuum is concerned the velocity gradient tensor can be considered as follows

$$(\operatorname{grad}\mathbf{v})_m = \nabla\mathbf{v}_m\mathbf{F}^{-1} = \dot{\mathbf{F}}\mathbf{F}^{-1} = \mathbf{D} + \mathbf{W}\,, \tag{2.19}$$

where the symmetric tensor $\mathbf{D} \in \mathbb{S}\mathtt{ym}$ and the skew part $\mathbf{W} \in \mathbb{S}\mathtt{kw}$ are respectively called the *stretching* and the *spin* tensors.

2.1.4 Distortions

Distortions of a body $\mathscr{B}$ of any part of it will be described by the tensor-valued field

$$\mathbf{F}_o : \mathscr{B} \to \mathbb{L}\mathtt{in}\,. \tag{2.20}$$

Then the *elastic deformation* $\mathbf{F}_e$ of the body elements can be introduced as the difference between the distortions $\mathbf{F}_o$ and the *visible* deformation $\mathbf{F}$ in the sense of a multiplicative decomposition

$$\mathbf{F}_e = \mathbf{F}\mathbf{F}_o^{-1}\,. \tag{2.21}$$

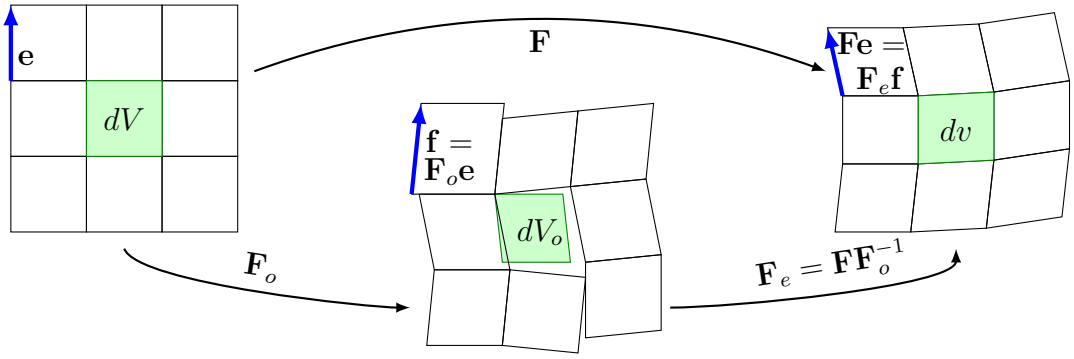

Figure 2.1: Illustrative example of a multiplicative decomposition of the deformation gradient in the flat 2D manifold.

It is worth noting that $\mathbf{F}_o$ and $\mathbf{F}_e$ are not, in general, gradients of any field. It means, therefore, that a general smooth field $\mathbf{F}_o$ can not be compatible, not even locally: volume elements in a neighbourhood of X can not match any longer once they have been distorted under $\mathbf{F}_o$. To stick together all the distorted elements, a further deformation $\mathbf{F}_e$ is needed, see figure 2.1. The stance after $\mathbf{F}_o$ has been applied to the reference configuration can be called *distorted, relaxed, ground* or *rest state*. Let the right Cauchy–Green strain measures be defined in terms of distortion and elastic deformation

$$\mathbf{C}_e = \mathbf{F}_e^{\mathrm{T}}\mathbf{F}_e = \mathbf{F}_o^{-\mathrm{T}}\mathbf{C}\mathbf{F}_o^{-1} \quad \text{and} \quad \mathbf{C}_o = \mathbf{F}_o^{\mathrm{T}}\mathbf{F}_o\,. \tag{2.22}$$

It is worth noting that $\mathbf{C}_o$ measures the stretch λ_o undergone by a reference fibre $\mathbf{e}$ once embedded in the distorted state. In an similar way $\mathbf{C}_e$ measures the stretch λ_e undergone by a distorted fibre $\mathbf{f}$ in the actual state, see figure 2.1.

Therefore it is possible to write

$$\mathbf{e} \mapsto \mathbf{f} = \mathbf{F}_o \mathbf{e} \quad \text{thus} \quad \lambda_o^2 = \mathbf{C}_o \cdot \mathbf{e} \otimes \mathbf{e} = \mathbf{f} \cdot \mathbf{f} \tag{2.23}$$

and

$$\lambda_e^2 = \mathbf{C}_e \cdot \mathbf{f} \cdot \mathbf{f} = \mathbf{C} \cdot \mathbf{e} \otimes \mathbf{e} \,. \tag{2.24}$$

2.2 Dynamics

The basic concepts of stress in terms of distortions are explained in this chapter in subsection 2.2.3. It should be noted that the idea to associate the zero stress state to the distorted configuration was firstly introduced in (Rodriguez et al., 1994) and extended in terms of a constitutive theory in (DiCarlo and Quiligotti, 2002).

2.2.1 Balance and stress

Let the virtual velocity field be $\mathbf{v} \in V\mathscr{E}$, the set of all admissible functions over the closure of the body $\bar{\mathscr{B}}_t$ in the actual configuration and the system $(\mathbf{c}, \mathbf{d})$ of the *external* (contact) and *internal* (bulk, distance) forces respectively. Then the *external virtual power expended* on a body part $\mathscr{P}_t \subset \mathscr{B}_t$ during the motion by a force system $(\mathbf{c}, \mathbf{d})$ is defined as

$$\mathbf{v} \mapsto \Pi^{ext}(\mathscr{P}_t)[\mathbf{v}] := \int_{\partial \mathscr{P}_t} \mathbf{c} \cdot \mathbf{v} + \int_{\mathscr{P}_t} \mathbf{d} \cdot \mathbf{v} \,. \tag{2.25}$$

Given the *Cauchy stress* $\mathbf{T}$ on the body $\mathscr{B}_t$ then the *internal virtual power* is to be defined

$$\operatorname{grad} \mathbf{v} \mapsto \Pi^{int}(\mathscr{P}_t)[\operatorname{grad} \mathbf{v}] := \int_{\mathscr{P}_t} \mathbf{T} \cdot \operatorname{grad} \mathbf{v} \,. \tag{2.26}$$

When the balance

$$\Pi^{ext}(\mathscr{P}_t)[\mathbf{v}] = \Pi^{int}(\mathscr{P}_t)[\operatorname{grad} \mathbf{v}] \,, \quad \forall \mathscr{P}_t \subset \mathscr{B}_t \,, \; \forall \mathbf{v} \in V\mathscr{E} \,, \tag{2.27}$$

of the external and internal virtual power is requested, then the integral balance in the actual configuration is

$$\int_{\partial\mathscr{P}_t} \mathbf{c}\cdot\mathbf{v} + \int_{\mathscr{P}_t} \mathbf{d}\cdot\mathbf{v} = \int_{\mathscr{P}_t} \mathbf{T}\cdot\operatorname{grad}\mathbf{v}\,, \quad \forall\mathscr{P}_t\subset\mathscr{B}_t\,,\ \forall\mathbf{v}\in V\mathscr{E}\,. \tag{2.28}$$

Assuming the smoothness of a tensor valued field $\mathbf{T}$ over $\mathscr{B}_t$, then balance (2.28) can be expressed thanks to the *per partes* rule based on relation (A.3) and Stokes identity (A.4) at an arbitrary point of the body $\mathscr{B}_t$ as

$$\operatorname{div}\mathbf{T}+\mathbf{d}=\mathbf{0}\,, \quad \text{and} \quad \mathbf{c}=\mathbf{T}\mathbf{n}\,,\ \text{on}\ \mathscr{B}_t\,, \tag{2.29}$$

with $\mathbf{n}$ being the normal to $\partial\mathscr{P}_t$. It is worth noting that balance (2.28) in any arbitrary part $\mathscr{P}_t\subset\mathscr{B}_t$ can be written in the weaker form

$$\mathscr{P}_t\to\mathscr{B}_t:\ \int_{\partial\mathscr{B}_t} \mathbf{c}\cdot\mathbf{v} + \int_{\mathscr{B}_t} \mathbf{d}\cdot\mathbf{v} = \int_{\mathscr{B}_t} \mathbf{T}\cdot\operatorname{grad}\mathbf{v}\,, \quad \forall\mathbf{v}\in V\mathscr{E} \tag{2.30}$$

and in the same way as in relation (2.29) it is possible to derive the local form of (2.30) as follows

$$\begin{aligned} \operatorname{div}\mathbf{T}+\mathbf{d}&=\mathbf{0}\,, \quad \text{on}\ \mathscr{B}_t\,,\\ \mathbf{T}\mathbf{n}&=\mathbf{c}\,, \quad \text{on}\ \partial\mathscr{B}_t\,. \end{aligned} \tag{2.31}$$

It should be noted that the Cauchy stress is symmetric tensor $\mathbf{T}\in\mathbb{S}\mathtt{ym}$. This fact is implied by the statement that the internal virtual power is objective. For details see (Noll, 1963; Podio-Guidugli, 2000, 2009).

Let the virtual velocity field be $\bar{\mathbf{v}}\in V\mathscr{E}$ over the closure of the body $\bar{\mathscr{B}}$ and the force system $(\bar{\mathbf{c}},\bar{\mathbf{d}})$ in the reference configuration. Then the balance of the external and internal virtual power on the reference body part $\mathscr{P}$ is

$$\begin{aligned} \Pi^{est}(\mathscr{P})[\bar{\mathbf{v}}] &:= \int_{\partial\mathscr{P}} \bar{\mathbf{c}}\cdot\bar{\mathbf{v}} + \int_{\mathscr{P}} \bar{\mathbf{d}}\cdot\bar{\mathbf{v}} = \\ &= \int_{\mathscr{P}} \mathbf{S}\cdot\nabla\bar{\mathbf{v}} =: \Pi^{int}(\mathscr{P})[\nabla\bar{\mathbf{v}}]\,,\ \forall\mathscr{P}\subset\mathscr{B}\,,\ \forall\bar{\mathbf{v}}\in V\mathscr{E} \end{aligned} \tag{2.32}$$

and in the local form as in balance (2.31) is

$$\begin{aligned} \operatorname{Div}\mathbf{S}+\bar{\mathbf{d}}&=\mathbf{0}\,, \quad \text{on } \mathscr{B}\,,\\ \mathbf{S}\mathbf{m}&=\bar{\mathbf{c}}\,, \quad \text{on } \partial\mathscr{B}\,, \end{aligned} \tag{2.33}$$

with $\mathbf{m}$ being the outer normal to the boundary $\partial\mathscr{B}$. Here the *first Piola–Kirchhoff (reference) stress* $\mathbf{S} \in \mathbb{L}\mathtt{in}$, in general, is not the symmetric tensor. The integral balance equations on $\mathscr{B}_t$ and $\mathscr{B}$ are related by the request

$$\Pi^{ext}(\mathscr{B}_t)[\mathbf{v}]-\Pi^{int}(\mathscr{B}_t)[\operatorname{grad}\mathbf{v}]=\Pi^{ext}(\mathscr{B})[\bar{\mathbf{v}}]-\Pi^{int}(\mathscr{B})[\nabla\bar{\mathbf{v}}]\,,\ \forall\mathbf{v},\bar{\mathbf{v}}\in V\mathscr{E}\,, \tag{2.34}$$

where the fields of virtual velocities in the reference and actual configuration are related by $\bar{\mathbf{v}}=\mathbf{v}\circ\boldsymbol{\chi}$. Therefore the quantities in proper configurations are related as follows

$$\begin{aligned} \mathbf{S}&=\mathbf{T}\mathbf{F}^{\star}\,, & \mathbf{T}&=J^{-1}\mathbf{S}\mathbf{F}^{\mathrm{T}}\,,\\ \mathbf{d}&=J\bar{\mathbf{d}}\,, & \bar{\mathbf{d}}&=J^{-1}\mathbf{d}\,,\\ \mathbf{c}&=\|\mathbf{F}^{\star}\mathbf{m}\|\bar{\mathbf{c}}\,, & \bar{\mathbf{c}}&=\|\mathbf{F}^{\star}\mathbf{m}\|^{-1}\mathbf{c}\,. \end{aligned} \tag{2.35}$$

2.2.2 Energy and stress

In the following section the concept of hyperelasticity will be introduced and in that context the constitutive laws will be settled. The importance of these relations is shown by the fact that it is impossible to determine nine unknowns regarding the displacement $\mathbf{u}$ and the Cauchy stress $\mathbf{T}$ using balance (2.31) only. The natural conditions from which the constitutive equations are derived can be found in literature specialised in continuum mechanics, e.g. (Beatty, 1987; Ogden, 1997; Rosenberg and Křen, 1995).

In the *hyperelastic* theory every solid is characterized by the *strain energy* function defined on the space of deformation gradients $\mathbf{F} \in \mathbb{L}\mathtt{in}^{+}$

$$\psi(X,t)=\psi(\mathbf{F}(X,t),X,t)\,, \tag{2.36}$$

where ψ can also be called *elastic potential energy* or *stored energy* referred to be in a deformation gradient per unit reference volume, see (Beatty, 1987; Podio-Guidugli, 2000). From now on an argument of ψ will be automatically considered

and generally omitted, on the contrary only for the special cases will be specified. It should be noted that when $\mathscr{B}$ is a the stress free configuration, then it is referred to as a natural configuration for any unconstrained material and holds

$$\psi(\mathbf{I}) = 0\,, \quad \frac{\partial \psi}{\partial \mathbf{F}}(\mathbf{I}) = \mathbf{0}\,. \tag{2.37}$$

As in (Beatty, 1987; Podio-Guidugli, 2000) the total stored energy of *elastic material* is conserved, hence as far as the stress power is concerned the following holds

$$\Pi(\mathscr{P}) = (\int_{\mathscr{P}} \psi)^{\cdot} \tag{2.38}$$

and the first Piola–Kirchhoff stress tensor is expressed as

$$\mathbf{S} = \frac{\partial \psi}{\partial \mathbf{F}}\,. \tag{2.39}$$

Every elastic energy is required to be independent of superimposed body motions (principle of objectivity or frame indifference). Therefore $\psi(\mathbf{QF}) = \psi(\mathbf{F})$ is valid for all rotations $\mathbf{Q} \in \mathbb{O}\mathtt{rt}$. Using this principle it is possible to show that the stored energy can be expressed in terms of other deformation measures

$$\psi(\mathbf{F}) = \psi_C(\mathbf{C}) = \psi_B(\mathbf{B}) = \psi_E(\mathbf{E})\,, \tag{2.40}$$

see (Beatty, 1987; Ogden, 1997). Further restriction on the material symmetry in the reference configuration $\mathscr{B}$ is identified therein by transformations which do not affect the material response. When the symmetry group of the material relative to $\mathscr{B}$ is the proper orthogonal group, then it will be called *isotropic* and hold

$$\psi(\mathbf{FQ}) = \psi(\mathbf{F})\,, \tag{2.41}$$

for all rotations $\mathbf{Q} \in \mathbb{O}\mathtt{rt}$. This symmetry condition is naturally respected by using the principal invariants defined

$$I_1 = \mathbf{I} \cdot \mathbf{C}\,, \quad I_2 = \frac{1}{2}(I_1^2 - \mathbf{C}^2 \cdot \mathbf{I})\,, \quad I_3 = \det \mathbf{C}\,, \tag{2.42}$$

It should be noted that the values of the invariants are the same using the deformation tensor $\mathbf{B}$ instead of $\mathbf{C}$. The relations between the corresponding first

Piola–Kirchhoff and the Cosserat stress tensors can be derived from the definition of the *stress power* that is

$$\Pi(\mathscr{P}) = \int_{\mathscr{P}_t} \mathbf{T} \cdot \nabla \mathbf{v} = \int_{\mathscr{P}} \overbrace{\frac{\partial \psi}{\partial \mathbf{F}}}^{\mathbf{S}} \cdot \dot{\mathbf{F}} = \int_{\mathscr{P}} \overbrace{\frac{\partial \psi_E}{\partial \mathbf{E}}}^{\mathbf{S}_E} \cdot \dot{\mathbf{E}} = \int_{\mathscr{P}} \overbrace{\frac{\partial \psi_C}{\partial \mathbf{C}}}^{\mathbf{S}_C} \cdot \dot{\mathbf{C}}\,, \tag{2.43}$$

where $\mathbf{v} = \dot{\boldsymbol{\chi}}$ is the velocity of motion. The stresses $\mathbf{S} \in \mathbb{L}\mathtt{in}$ and $\mathbf{S}_E, \mathbf{S}_C \in \mathbb{S}\mathtt{ym}$ can be called the energetic stress measures and the following relation holds

$$\mathbf{S} = \mathbf{F}\mathbf{S}_E = 2\mathbf{F}\mathbf{S}_C\,. \tag{2.44}$$

For further details see (Beatty, 1987; Podio-Guidugli, 2000).

2.2.3 Incompressibility

During the deformation of an elastic solid a specific class of dynamic processes can be imposed. This restriction on the motion is called *internal constraint* and can be for example an invariant angle or consist in preserving volume deformations as it will be shown in this work. Due to the property of symmetry of the Cauchy stress tensor $\mathbf{T} \in \mathbb{S}\mathtt{ym}$ it is possible to perform an additive decomposition into a *deviatoric* $\operatorname{dev}\mathbf{T}$ part and a *spherical* $\operatorname{sph}\mathbf{T}$ part, where the second one plays a role in the reactive part of the stress and produces a zero stress power in every motion compatible with the internal constraint. From the incompressibility it can be deduced

$$\det \mathbf{F} = 1 \;\Rightarrow\; \operatorname{div}\mathbf{v} = 0. \tag{2.45}$$

Thereforeas far as the stress power is concerned:

$$\int_{\mathscr{P}_t} \mathbf{T} \cdot \operatorname{grad}\mathbf{v} = \int_{\mathscr{P}_t} \operatorname{dev}\mathbf{T} \cdot \operatorname{grad}\mathbf{v}\,, \tag{2.46}$$

and Cauchy stress can be decomposed as follows

$$\mathbf{T} = \operatorname{dev}\mathbf{T} + \operatorname{sph}\mathbf{T} = \operatorname{dev}\mathbf{T} + \frac{1}{3}(\operatorname{tr}\mathbf{T})\mathbf{I} = \operatorname{dev}\mathbf{T} - p\mathbf{I}\,. \tag{2.47}$$

The spherical reactive stress $\mathbf{T}_s = -p\mathbf{I}$ remains indeterminated because of the constant p, which is called *internal (hydrostatic) pressure*. For further details see (Beatty, 1987; Podio-Guidugli, 1994). An example of an isotropic homogeneous incompressible material is *neo-Hooke* with the following strain energy function

$$\psi = \frac{1}{2}\mu(I_1 - 3)\,, \tag{2.48}$$

where μ represents the shear modulus. It is worth noting that this is a special case of the *Mooney–Rivlin* or *Blatz–Ko* material description, see (Beatty, 1987).

In the context of a multiplicative decomposition of the deformation gradient $\mathbf{F}$ different stress measures can be attributed to proper states as it is sketched in figure 2.2. Apart from the Cauchy and the first Piola–Kirchhoff stress measures let the ground stress $\mathbf{S}_o$ be introduced in the distorted stance related to the other ones

$$\mathbf{S} = \mathbf{T}\mathbf{F}^\star = \mathbf{S}_o\mathbf{F}_o^\star\,. \tag{2.49}$$

The hyperelastic response of a body is assumed to be described by a strain energy density per unit ground volume ψ_o whose value at each body point $X \in \mathscr{B}$ depends only on the present value of the elastic deformation $\mathbf{F}_e$ at that point. In case of incompressibility of the material the following holds

$$\psi_o : \mathbf{F}_e \mapsto \psi_o(\mathbf{F}_e)\,, \quad \text{and} \quad J_e = \det(\mathbf{F}_e) = 1\,. \tag{2.50}$$

When the relation of the strain energy ψ per unit reference volume to ψ_o is defined by $\psi = J_o\psi_o$, with $J_o = \det \mathbf{F}_o$, then the energetic stress related to the distorted stance is

$$\mathbf{S}_o = \frac{\partial \psi_o}{\partial \mathbf{F}_e}\,, \quad \text{and} \quad \mathbf{S}_e = \mathbf{S}_o\mathbf{F}_o^\star\,. \tag{2.51}$$

In case of incompressibility the results for the first Piola–Kirchhoff and the Cauchy stress measures are

$$\mathbf{S} = \mathbf{S}_e - p\mathbf{F}^\star\,, \quad \text{and} \quad \mathbf{T} = \mathbf{S}_e(\mathbf{F}^\star)^{-1} - p\mathbf{I}\,. \tag{2.52}$$

It should be noted that from the time derivative of the strain energy ψ and the

relation $\psi = J_o \psi_o$, as in (2.43), relation (2.51) applies, thus

$$\dot{\psi} = \overbrace{\frac{\partial \psi}{\partial \mathbf{F}}}^{\mathbf{S}_e} \cdot \dot{\mathbf{F}} = J_o \frac{\partial \psi_o}{\partial \mathbf{F}_e} \cdot \dot{\mathbf{F}}_e = \overbrace{\frac{\partial \psi_o}{\partial \mathbf{F}_e}}^{\mathbf{S}_o} \mathbf{F}_o^{\star} \cdot \dot{\mathbf{F}} \,. \tag{2.53}$$

In the same way as for the stress power in (2.43) the following can be derived from the time derivative of the strain energy

$$\dot{\psi}_o = \frac{\partial \psi_o}{\partial \mathbf{C}_e} \cdot \dot{\mathbf{C}}_e = \frac{\partial \psi_o}{\partial \mathbf{F}_e} \cdot \dot{\mathbf{F}}_e \,, \tag{2.54}$$

the relation for the energetic stresses being then

$$\mathbf{S}_o = \frac{\partial \psi_o}{\partial \mathbf{F}_e} = 2\mathbf{F}_e \frac{\partial \psi_o}{\partial \mathbf{C}_e} \,. \tag{2.55}$$

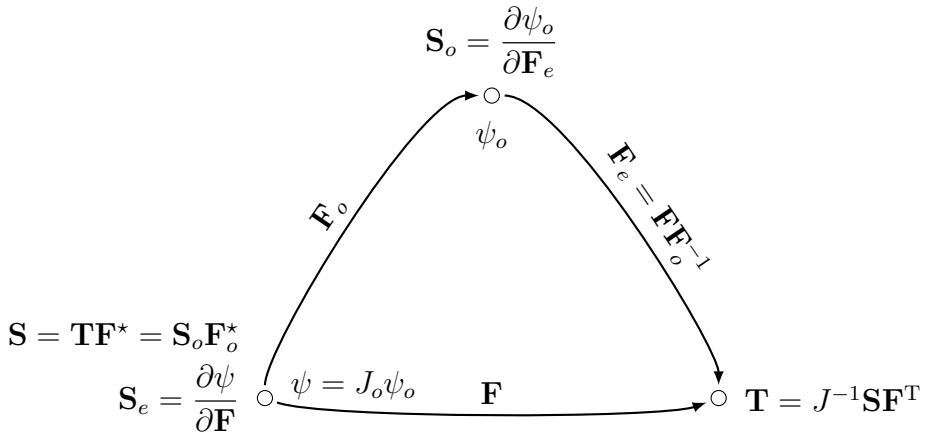

Figure 2.2: Deformation gradient decomposition with sketched stresses and strain energies.

In order to improve the computational performance, the nearly incompressibility is introduced. It consists in the multiplicative decomposition of the elastic deformation tensor $\mathbf{F}_e$ into the *isochoric (spherical)* $\bar{\mathbf{F}}_e$ part and the *deviatoric (volumetric, dilatation)* $J_e^{\frac{1}{3}}\mathbf{I}$ part of the elastic deformation

$$\mathbf{F}_e = J_e^{\frac{1}{3}} \bar{\mathbf{F}}_e \,, \quad \text{and} \quad \det \bar{\mathbf{F}}_e = 1 \,. \tag{2.56}$$

The relaxed strain energy, like in (Flory, 1961), is therefore additively decomposed into the isochoric and the volumetric part

$$\psi_o = \psi_{iso}(\bar{\mathbf{C}}_e) + \psi_{vol}(J_e)\,. \tag{2.57}$$

As far as $\psi = J_o\psi_o$ is concerned, its time rate can be derived as follows

$$\dot{\psi} = J_o\frac{\partial\psi_{iso}}{\partial\mathbf{F}_e}\cdot\dot{\mathbf{F}}_e + J_o\frac{\partial\psi_{vol}}{\partial J_e}\cdot\dot{J}_e = (\frac{\partial\psi_{iso}}{\partial\mathbf{F}_e}\mathbf{F}_o^{\star} + \frac{\partial\psi_{vol}}{\partial J_e}\mathbf{F}^{\star})\cdot\dot{\mathbf{F}}\,. \tag{2.58}$$

The previous expression identifies a constitutive relation for the whole first Piola–Kirchhoff stress $\mathbf{S}$ as a sum of the isochoric and volumetric contribution

$$\mathbf{S} = \mathbf{S}_{iso} + \mathbf{S}_{vol}\,, \quad \text{with} \quad \mathbf{S}_{iso} = \frac{\partial\psi_{iso}}{\partial\mathbf{F}_e}\mathbf{F}_o^{\star}\,, \quad \text{and} \quad \mathbf{S}_{vol} = -p\mathbf{F}^{\star}\,, \tag{2.59}$$

where the internal pressure is determined as

$$p = -\frac{\partial\psi_{vol}}{\partial J_e}\,, \tag{2.60}$$

and the isochoric term is determined from the time rate of the isochoric part of the relaxed strain energy

$$\dot{\psi}_{iso} = J_e^{-\frac{1}{3}}(\frac{\partial\psi_{iso}}{\partial\bar{\mathbf{F}}_e} - \frac{1}{3}(\frac{\partial\psi_{iso}}{\partial\bar{\mathbf{F}}_e}\cdot\mathbf{F}_e)\mathbf{F}_e^{-\mathrm{T}})\cdot\dot{\mathbf{F}}_e = \frac{\partial\psi_{iso}}{\partial\mathbf{F}_e}\cdot\dot{\mathbf{F}}_e\,. \tag{2.61}$$

Therefore from the previous relations, namely for the neo-Hookean material the first Piola–Kirchhoff and Cauchy stresses are

$$\mathbf{S} = \mu J_o^{\frac{5}{3}}J^{-\frac{2}{3}}(\mathbf{F}\mathbf{C}_o^{-1} - \frac{1}{3}(\mathbf{C}\cdot\mathbf{C}_o^{-1})\mathbf{F}^{-\mathrm{T}}) - p\mathbf{F}^{\star}\,, \tag{2.62}$$

and

$$\mathbf{T} = \mu J_o^{\frac{5}{3}}J^{-\frac{5}{3}}(\mathbf{F}\mathbf{C}_o\mathbf{F}^T - \frac{1}{3}(\mathbf{C}\cdot\mathbf{C}_o^{-1})\mathbf{I}) - p\mathbf{I}\,. \tag{2.63}$$

The internal hydrostatic pressure prescribed by the choice of volumetric part of the strain energy

$$\psi_{vol}(J_e) = \frac{1}{2}\kappa(J_e - 1)^2\,, \tag{2.64}$$

hence it is

$$p = -\kappa(J_e - 1)\,. \tag{2.65}$$

Here κ is the bulk modulus. Note that this volumetric function is not the unique possible choice for the tackling incompressibility, see (Hartmann and Neff, 2006).

2.2.4 Active strain vs active stress

The construction of the model that describes the response of soft living tissues to the deformation can be performed in two ways. In the first one, the active strain approach, the distortion $\mathbf{F}_o$ is introduced by (2.20) and consequently used to define the stress-free state of the material, which may be activated by coupling it to some external event, e.g. an electrochemical reaction. For an illustration see figures 2.3 and 2.1. The other way the active stress can be an addition of an active stress to the Cauchy stress expressing the passive part as follows

$$\mathbf{T} = \frac{\partial \psi}{\partial \mathbf{F}}(\mathbf{F}^\star)^{-1} + \mathbf{T}_a\,, \tag{2.66}$$

where the active stress $\mathbf{T}_a$ is, in general, a function of deformation gradient $\mathbf{F}$. For variety of $\mathbf{T}_a$ see for example (Ambrosi and Pezzuto, 2011).

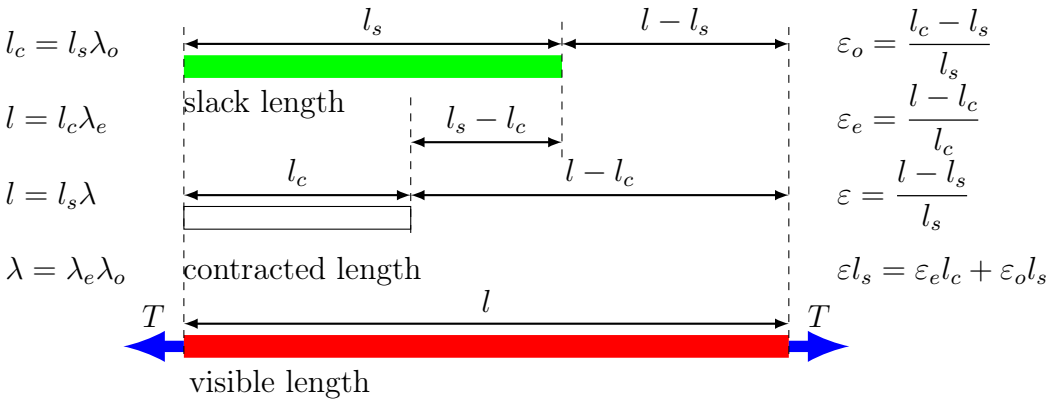

Figure 2.3: A one-dimensional example of active strain illustrating the modelling of soft tissue. The fiber of tissue in the reference state (green) has length l_s, which is contracted to the length l_c in the distorted stance (white), then the traction T has to be applied to obtain the visible deformation of the fiber long l embedded in the actual configuration (red).

To show the difference between the active stress and the active strain is not an easy task. A one dimensional illustration can be found in figure 2.3. Note that from the mathematical point of view the active strain description is more robust than the active stress approach especially as far as maintaining the rank of ellipticity condition or frame invariance is concerned, see (Ambrosi and Pezzuto, 2011; Cherubini et al., 2008; Nardinocchi and Teresi, 2007; Rossi et al., 2012) for further discussion.

Chapter 3

Numerical methods

3.1 Functional spaces

Let the Lebesgue space of measurable functions be defined on a domain $\mathscr{B}$, which is Lebesgue measurable open subset of $\mathbb{R}^n$ with non empty interior,

$$L^2(\mathscr{B}) := \{u : \ \|u\|_{L^2(\mathscr{B})} < \infty\}, \tag{3.1}$$

where the norm of a real valued Lebesgue measurable function $u(x)$ defined on $\mathscr{B}$ is

$$\|u\|_{L^2(\mathscr{B})} := (\int_{\mathscr{B}} |u(x)|^2 \, dx)^{\frac{1}{2}}. \tag{3.2}$$

Let

$$(u, v)_{L^2(\mathscr{B})} := (\int_{\mathscr{B}} u(x)v(x))^{\frac{1}{2}} \tag{3.3}$$

represent a scalar product in the space $L^2(\mathscr{B})$, then the inner product space (Sobolev space) can be introduced as follows

$$H^k(\mathscr{B}) := \{u \in L_{loc}(\mathscr{B}) : \|u\|_{H^k(\mathscr{B})} < \infty\}, \tag{3.4}$$

with a norm

$$\|u\|_{H^k(\mathscr{B})} := (\sum_{|\alpha| \leq k} (D^\alpha u, D^\alpha u)^2_{L^2(\mathscr{B})})^{\frac{1}{2}}. \tag{3.5}$$

Here α denotes a multi-index and $L^1_{loc}(\mathscr{B})$ represents a space of locally integrable functions on all compact interior subsets of $\mathscr{B}$. For the details see (Brenner and

Scott, 2007). The solution of variational problems is usually looked for in the following spaces

$$V := \{v \in H^1(\mathscr{B}) : \ v = 0 \text{ on } \partial_k \mathscr{B}\} \quad \text{and} \quad M := \{v \in \ L^2(\mathscr{B})\}, \tag{3.6}$$

where $\partial_k \mathscr{B}$ is a part of boundary with the imposed kinematic boundary conditions $u = \bar{u}$. It is worth noting that in literature the space V is also denoted as $H_0^1(\mathscr{B})$.

3.2 Finite element spaces

For the formulation of the finite element methods, namely the Galerkin and the discontinuous Galerkin methods as far as the proper variational problems are concerned, there is a request of weighted finite element subspaces V_h of spaces V. As it is shown in (Johnson, 2009; Křížek and Neittaanmäki, 1990), to define them, the following conditions have to be specified:

- the triangulation T_h is established over the domain $\bar{\mathscr{B}}$,
- the nature of the functions v_h in the space V_h is piecewise polynomial,
- the basis with a small support does exist in the space V_h.

The triangulation T_h is the division of the set $\bar{\mathscr{B}}$ into a finite number of subsets called elements K which have the following properties:

- the union of all elements K of triangulation T_h yields the subdivided set $\bar{\mathscr{B}} = \bigcup_{K \in T_h} K$,
- each set K of triangulation T_h is closed and its interior K^0 is non-empty,
- each distinct K_1, $K_2 \in T_h$ have no intersection that is $K_1^0 \cap K_2^0 = \emptyset$,
- each element $K \in T_h$ has the Lipschitz boundary ∂K.

It should be noted that h, the maximum diameter of all $K \in T_h$, as a lower index, is connected with a discretized domain. When two or three dimensions are considered, then

- any face of any $K \in T_h$ is either a subset of the boundary $\partial\mathscr{B}$, or a face of any other element $K' \in T_h$,

- the interior of any face of any $K \in T_h$ is disjoint with the set of points where one type of boundary condition changes into another – the consistency condition, see (Křížek and Neittaanmäki, 1990).

It is worth noting that the set K of the triangulation T_h will be considered as a simplex so that in one, two or three dimensions it will be respectively a line, a triangle or a tetrahedron. To specify the nature of the functions of V_h let us define the finite element by the triple (K, P, Σ), where

- $K \neq 0$ is a closed subset of $\mathbb{R}$, $\mathbb{R}^2$ or $\mathbb{R}^3$ with a Lipschitz boundary

- P is a space of real-valued functions defined over the set K

- Σ is a finite set of linearly independent linear forms $\Phi_1, \ldots, \Phi_N$ defined over the space P or over a space which contains P.

Here P denotes the space of all polynomials called ansatz-functions.

Lagrange linear element

The set P of the linear Lagrange element is the set of polynomials of degree one

$$P_1(K) = \{p_1(x, y) = a_0 + a_1 x + a_2 y\,,\ a_i \in \mathbb{R}\,,\ i = 0, 1, 2\} \tag{3.7}$$

and the set of degrees of freedom Σ of the linear Lagrange element is

$$\Sigma_1(K) = \{p_1(A_i),\ 1 \leqslant i \leqslant 3\}\,, \tag{3.8}$$

where A_i are the vertices of the simplex K.

Lagrange quadratic element

The set P of the second degree Lagrange element are polynomials of degree two

$$P_2(K) = \{p_2(x, y) = a_0 + a_1 x + a_2 y + a_{11} x^2 + a_{12} xy + a_{22} y^2,\ a_i, a_{ij} \in \mathbb{R}\} \tag{3.9}$$

and the set of degrees of freedom Σ of the quadratic Lagrange element will be

$$\Sigma_2(K) = \{p_2(A_i),\ 1 \leqslant i \leqslant 3;\ p_2(A_{ij}),\ 1 \leqslant i < j \leqslant 3\}\,, \tag{3.10}$$

where $A_{ij} = 1/2(A_i + A_j)$ are the midpoints of edges of simplex K.

The spaces of the weighted functions V_h can be defined for the linear Lagrange elements as

$$V_h = \{v :\ v|_K \in P_1(K)\ \forall K \in T_h \text{ and is continuous at the nodes}\} \tag{3.11}$$

and for the quadratic Lagrange elements as

$$V_h = \{v \in C^0(\bar{\mathscr{B}}) :\ v|_K \in P_2(K),\ \forall K \in T_h\}\,. \tag{3.12}$$

When continuity in the space of all integrable functions M is required, then its weighted subspace will be denoted M_h. When the weighted subspace of M with no continuity requirements accross interelement boundaries is equipped by the first or the second order Lagrange element, then it can be defined

$$W_h := \{v \in L^2(\mathscr{B}) :\ v|_K \in P_r(K)\ \forall K \in T_h\}\,, \tag{3.13}$$

where $P_r(K)$ are the polynoms on K of degree at most r, here $r = 1, 2$.

Remark 1. It is worth noting that later on, the Lagrange elements associated with the weighted space W_h will be called *discontinuous elements* and the nomination *Lagrange elements* will be reserved for those associated with the weighted space V_h. The first and the second order Lagrange elements will be respectively called Lag_1 and Lag_2. And the first and the second order discontinuous elements will be respectively defined as Dsc_1 and Dsc_2.

Remark 2. In two or three dimensions, when two or three spatial variables appear, then the variational space is called $[V]^d$, where $1 \leqslant d \leqslant 3$ is the spatial dimension. As far as the complicated kinematic conditions are concerned the

usual convention on the variational space does apply as follows

$$\begin{aligned}[V]^d := \{\mathbf{u} \in [H^1(\mathscr{B})]^d : \ & \mathbf{u} \text{ satisfies the admissible kinematic BC} \\ \text{and } \tilde{\mathbf{u}} \in [H^1(\mathscr{B})]^d : \ & \text{is compatible with such kinematic BC}\} .\end{aligned} \tag{3.14}$$

For further details see (Braess, 2007).

3.3 Finite element methods

For the derivation of a various type of finite element methods, several procedures are used and the basic scheme in figure 3.1 describes the relations between these procedures. Further information about the relations between proper formulations can be found in (Johnson, 2009)

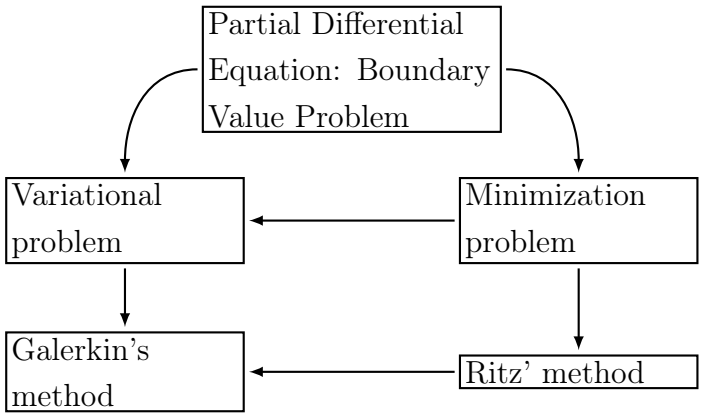

Figure 3.1: Standard procedures for the derivation of numerical schemes.

The following text is based on the scheme in figure 3.1 and demonstrates the derivation of the numerical schemes used in chapter 4. Consider a boundary value problem of non linear finite elasticity (2.33) stating:

"Find the displacement field $\mathbf{u}$ so that the following equations hold

$$\begin{aligned} \operatorname{Div} \mathbf{S} + \mathbf{d} &= \mathbf{0} \quad \text{in } \mathscr{B} \\ \mathbf{S}\mathbf{m} &= \mathbf{c} \quad \text{on } \partial_d \mathscr{B} \\ \mathbf{u} &= \bar{\mathbf{u}} \quad \text{on } \partial_k \mathscr{B} , \end{aligned} \tag{3.15}$$

where the material is hyperelastic and the dependance of the first Piola–Kirchhoff stress tensor $\mathbf{S}$ on the displacement field $\mathbf{u}$ is derived from (2.49), (2.51) and (2.52)."

The classical solution $\mathbf{u}$ of this problem is usually numerically found thanks to other formulations. Hence like in chapter 2, when the equation (3.15) is multiplied by $\tilde{\mathbf{u}}$ and when the *per partes* integration is applied, involving rule (A.3) and Stokes identity (A.4), then the variational problem can be defined as:

"Find the displacement field $\mathbf{u}$ so that that following relation holds

$$\int_{\mathscr{B}} (\operatorname{Div} \mathbf{S} + \mathbf{d}) \cdot \tilde{\mathbf{u}} = -\int_{\mathscr{B}} \mathbf{S} \cdot \nabla \tilde{\mathbf{u}} + \int_{\mathscr{B}} \mathbf{d} \cdot \tilde{\mathbf{u}} + \int_{\partial_d \mathscr{B}} \mathbf{c} \cdot \tilde{\mathbf{u}} = 0 \quad \forall \tilde{\mathbf{u}} \in [V]^d\,, \tag{3.16}$$

where the kinematic boundary conditions $\mathbf{u} = \bar{\mathbf{u}}$ are fulfilled on $\partial_k \mathscr{B}$."

As it is sketched in the scheme from figure 3.1 the variational problem (3.16) can be derived from the minimization problem that is:

"Find the displacement field $\mathbf{u}$ such that

$$\Pi(\mathbf{u}) := -\int_{\mathscr{B}} \psi(\mathbf{F}(\mathbf{u})) + \int_{\mathscr{B}} \mathbf{d} \cdot \mathbf{u} + \int_{\partial_d \mathscr{B}} \mathbf{c} \cdot \mathbf{u} \tag{3.17}$$

is a global minimum

$$\Pi(\mathbf{u}) = \min_{\tilde{\mathbf{u}}} \Pi(\tilde{\mathbf{u}}) \quad \forall \tilde{\mathbf{u}} \in [V]^d\,." \tag{3.18}$$

The variation is defined by the Gâteaux derivative, which due to fact that $\tilde{\mathbf{F}} = \nabla \tilde{\mathbf{u}}$ can be read:

$$\begin{aligned} \delta\Pi(\mathbf{u})[\tilde{\mathbf{u}}] &= \frac{d}{d\varepsilon}(\Pi(\mathbf{u} + \varepsilon\tilde{\mathbf{u}}))|_{\varepsilon=0} = \\ &= -\int_{\mathscr{B}} \frac{\partial \psi}{\partial \mathbf{F}} \cdot \nabla \tilde{\mathbf{u}} + \int_{\mathscr{B}} \mathbf{d} \cdot \tilde{\mathbf{u}} + \int_{\partial_d \mathscr{B}} \mathbf{c} \cdot \tilde{\mathbf{u}} = 0 \quad \forall \tilde{\mathbf{u}} \in [V]^d\,, \end{aligned} \tag{3.19}$$

where the stress is defined in (2.39). If the finite space V_h is considered, then both variational problems (3.16) and (3.19) are called *compatible methods*. As

shown in (Bathe, 1996) if the compatible formulation (3.16) is used, the computations yield the locking effect or there can even be no convergence to the solution. That is why the mixed finite element schemes are introduced. The theory of this kind of schemes is further analysed in (Brezzi and Fortin, 1991; Hughes, 1987; Wriggers, 2008; Zienkiewicz et al., 2009).

Mixed method:
To avoid the computational difficulties the proposed mixed displacement–pressure formulation does apply. Consider the additive decomposition of the strain energy function (2.57) and the functional

$$\Pi(\mathbf{u},p) = -\int_{\mathscr{B}} (\psi_{iso}(\mathbf{u}) + \psi_{vol}(\mathbf{u},p)) + \frac{1}{2}\int_{\mathscr{B}} \frac{p^2}{2\kappa} + \int_{\mathscr{B}} \mathbf{d}\cdot\mathbf{u} + \int_{\partial\mathscr{B}} \mathbf{c}\cdot\mathbf{u}\,, \quad (3.20)$$

$$\psi_{vol} = \frac{1}{2}\kappa(J-1)^2 = -\frac{p}{2}(J-1) \quad \text{and} \quad p = -\kappa(J-1)\,, \quad (3.21)$$

$$\begin{aligned}\delta\Pi(\mathbf{u},p)[\tilde{\mathbf{u}}] = -\int_{\mathscr{B}} (\frac{\partial\psi_{iso}}{\partial\mathbf{F}} + \frac{d\psi_{vol}}{dJ} J\mathbf{F}^{-\mathrm{T}})\cdot\nabla\tilde{\mathbf{u}} + \\ + \int_{\mathscr{B}} \mathbf{d}\cdot\tilde{\mathbf{u}} + \int_{\partial\mathscr{B}} \mathbf{c}\cdot\tilde{\mathbf{u}} = 0 \quad \forall\tilde{\mathbf{u}}\in[V]^d\end{aligned} \quad (3.22)$$

$$\delta\Pi(\mathbf{u},p)[\tilde{p}] = \frac{1}{2}\int_{\mathscr{B}} (\frac{p}{\kappa} + J - 1)\tilde{p} = 0 \quad \forall\tilde{p}\in M \quad (3.23)$$

Therefore the mixed method states:

"Find the couple $(\mathbf{u},p)\in[V_h]^d\times M_h$ so that the weak forms (3.22–3.23) hold for all the couples $(\tilde{\mathbf{u}},\tilde{p})\in[V_h]^d\times M_h$."

It should be noted that the mixed displacement–pressure formulation is also very often used, by the weak term for the third variable regarding Jacobian. The use of it has been ommited in this work, because the same results do apply with the mixed method (3.22–3.23) For further details see (Simo and Taylor, 1991; Wriggers, 2008).

De Veubeke–Hu–Washizu method:
The de Veubeke–Hu–Washizu (dVHW) formulation known also as the method of H.C. Hu and K. Washizu was initially introduced by B.M.F. de Veubeke[1] in 1951, for further details see (Braess, 2007; de Veubeke, 1951; Hu, 1954; Jihuan, 1997; Washizu, 1974). Like in (Wriggers, 2008) let the following functional be looked at

$$\Pi(\boldsymbol{\chi}, \mathbf{F}, \mathbf{S}) = \int_{\mathscr{B}} (\psi(\mathbf{F}) + \mathbf{S} \cdot (\nabla\boldsymbol{\chi} - \mathbf{F})) + \int_{\mathscr{B}} \mathbf{d} \cdot \boldsymbol{\chi} + \int_{\partial\mathscr{B}} \mathbf{c} \cdot \boldsymbol{\chi} \tag{3.24}$$

Considering that $\tilde{\boldsymbol{\chi}} = \tilde{\mathbf{u}}$ holds, the first variation of the functional, as far as its variables are concerned yields

$$\delta\Pi(\boldsymbol{\chi}, \mathbf{F}, \mathbf{S})[\tilde{\boldsymbol{\chi}}] = \int_{\mathscr{B}} (\mathbf{S}(\mathbf{F}, p) \cdot \nabla\tilde{\boldsymbol{\chi}} + \mathbf{d} \cdot \tilde{\boldsymbol{\chi}}) - \int_{\partial\mathscr{B}} \mathbf{c} \cdot \tilde{\boldsymbol{\chi}} = 0 \quad \forall\tilde{\mathbf{u}} \in [V]^d \tag{3.25}$$

$$\delta\Pi(\boldsymbol{\chi}, \mathbf{F}, \mathbf{S})[\tilde{\mathbf{S}}] = \int_{\mathscr{B}} (\nabla\boldsymbol{\chi} - \mathbf{F}(\mathbf{u})) \cdot \tilde{\mathbf{S}} = 0 \quad \forall\tilde{\mathbf{S}} \in [M]^{d^2} \tag{3.26}$$

$$\delta\Pi(\boldsymbol{\chi}, \mathbf{F}, \mathbf{S})[\tilde{\mathbf{F}}] = \int_{\mathscr{B}} (\frac{\partial\psi(\mathbf{F}, p)}{\partial\mathbf{F}} - \mathbf{S}(\mathbf{F}, p)) \cdot \tilde{\mathbf{F}} = 0 \quad \forall\tilde{\mathbf{F}} \in [M]^{d^2} \tag{3.27}$$

and the weak incompressibility (3.23) holds. Therefore the aim of the dVHW method remaines:

"Find a quartet $(\mathbf{u}, \mathbf{F}, \mathbf{S}, p) \in [V_h]^d \times [M_h]^{d^2} \times [M_h]^{d^2} \times M_h$ so that balances (3.25–3.27) and (3.23) hold for all quartets $(\tilde{\mathbf{u}}, \tilde{\mathbf{F}}, \tilde{\mathbf{S}}, \tilde{p}) \in [V_h]^d \times [M_h]^{d^2} \times [M_h]^{d^2} \times M_h$."

Remark 3. It is worth noting that the compatible, the mixed and the dVHW methods are of a Garekin's type if the elements are taken from the weight spaces M_h. In chapter 4 the weighted spaces W_h of discontinuous functions are introduced for the dVHW method. Such an approach is called the discontinuous Galerkin's method.

[1] Baudouin M. Fraeijs de Veubeke 1917–1976 was a Belgian scientist, an engineer and a university professor.

Chapter 4

Problem formulation and its analysis

A significant problem in the three dimensional frame will be established in the following chapter. Its expected behaviour is described in the simplified example here under, in which the numerical results obtained by the mixed method are briefly analysed. Then the reduction of its size is reached by introducing the plane strain problem and the various analyses are carried out. The mixed and dVHW method are tested and the results are then compared for various types of mesh. In a further analysis the uniaxial problem is introduced and its exact solution is found. The compatible, mixed and dVHW schemes are introduced in one space dimension and after that the computational results are compared with the analytical ones.

4.1 Three dimensional configuration

The mixed method for the decomposition of the deformation gradient (2.21) is

$$\int_{\mathscr{B}} (-\mathbf{S}(\mathbf{F}_e, p) \cdot \nabla \tilde{\mathbf{u}} + \mathbf{d} \cdot \tilde{\mathbf{u}}) - \int_{\partial\mathscr{B}} \mathbf{c} \cdot \tilde{\mathbf{u}} = 0 \;\&\; \mathbf{u} = \bar{\mathbf{u}} \text{ on } \partial\mathscr{B}_d\,,\ \forall \tilde{\mathbf{u}} \in [V]^3\,, \quad (4.1)$$

$$\int_{\mathscr{B}} (\frac{p}{\kappa} + J - J_o)\tilde{p} = 0\,, \quad \forall \tilde{p} \in M\,, \quad (4.2)$$

For the derivation of the numerical schemes, the formulation of the problem has been performed as a minimization of the potential functional. The variation in the deformation (placement) $\boldsymbol{\chi}$, the elastic deformation $\mathbf{F}_e$ and the reference stress $\mathbf{S}$ is followed when the dVHW method has been established. The reference (material) configuration is considered as the computational manifold. The general propounded functional without any regards to material properties is

$$\Pi(\boldsymbol{\chi}, \mathbf{F}_e, \mathbf{S}) = \int_{\mathscr{B}} (-J_o \psi_o(\mathbf{F}_e) - \mathbf{S} \cdot (\nabla \boldsymbol{\chi} - \mathbf{F}) + \mathbf{d} \cdot \boldsymbol{\chi}) + \int_{\partial \mathscr{B}} \mathbf{c} \cdot \boldsymbol{\chi}\,, \tag{4.3}$$

where the elastic energy ψ_o defined on the rest configuration is accounted in the reference domain and holds the relation $\psi(\mathbf{F}) = J_o \psi_o(\mathbf{F}_e)$. And the elastic deformation on the reference configuration takes account of a distortion as a part of the multiplicative decomposition of the deformation gradient $\mathbf{F} = \mathbf{F}_e \mathbf{F}_o$. When the first variation of the functional (4.3) in the space determined by the elements $\tilde{\boldsymbol{\chi}}$, $\tilde{\mathbf{F}}_e$ and $\tilde{\mathbf{S}}$ is performed, then the following expression holds

$$\begin{aligned} \delta\Pi(\boldsymbol{\chi}, \mathbf{F}_e, \mathbf{S})[\tilde{\boldsymbol{\chi}}, \tilde{\mathbf{F}}_e, \tilde{\mathbf{S}}] = \int_{\mathscr{B}} (-J_o \frac{\partial \psi_o}{\partial \mathbf{F}_e} \cdot \tilde{\mathbf{F}}_e - \mathbf{S} \cdot (\nabla \tilde{\boldsymbol{\chi}} - \tilde{\mathbf{F}}_e \mathbf{F}_o)) \\ - \int_{\mathscr{B}} ((\nabla \boldsymbol{\chi} - \mathbf{F}) \cdot \tilde{\mathbf{S}} - \mathbf{d} \cdot \tilde{\boldsymbol{\chi}}) + \int_{\partial \mathscr{B}} \mathbf{c} \cdot \tilde{\boldsymbol{\chi}}\,. \end{aligned} \tag{4.4}$$

Then comparing (4.4) to zero, these three balances are obtained

$$\int_{\mathscr{B}} (-\mathbf{S}(\mathbf{F}_e, p) \cdot \nabla \tilde{\boldsymbol{\chi}} + \mathbf{d} \cdot \tilde{\boldsymbol{\chi}}) + \int_{\partial \mathscr{B}} \mathbf{c} \cdot \tilde{\boldsymbol{\chi}} = 0\,, \quad \text{for all } \tilde{\boldsymbol{\chi}} = \tilde{\mathbf{u}} \in [V]^d\,, \tag{4.5}$$

$$\int_{\mathscr{B}} (\mathbf{S}(\mathbf{F}_e, p) \mathbf{F}_o^{\mathrm{T}} - J_o \frac{\partial \psi_o(\mathbf{F}_e, p)}{\mathbf{F}_e}) \cdot \tilde{\mathbf{F}}_e = 0\,, \quad \text{for all } \tilde{\mathbf{F}}_e \in [M]^{d^2}\,, \tag{4.6}$$

$$\int_{\mathscr{B}} (\mathbf{F}_e(\mathbf{u}) \mathbf{F}_o - \nabla \boldsymbol{\chi}) \cdot \tilde{\mathbf{S}} = 0\,, \quad \text{for all } \tilde{\mathbf{S}} \in [M]^{d^2}\,. \tag{4.7}$$

They form the dVHW scheme for the generalized problems of non linear elasticity, where large distortions are tackled. When the slightly incompressibility is considered, the following weak form is added to the scheme, see (Wriggers, 2008)

$$\int_{\mathscr{B}} (p + \frac{d\psi_{vol}(J_e)}{dJ_e}) \tilde{p} = 0\,, \quad \text{for all } \tilde{p} \in M\,. \tag{4.8}$$

Therefore the formulation of the d-dimensional dVHW method for the problem of non linear elasticity with large distortions for the incompressible materials consists in finding the displacement $\mathbf{u} \in [V_h]^d$, the stress $\mathbf{S} \in [W_h]^{d^2}$, the elastic deformation $\mathbf{F}_e \in [W_h]^{d^2}$ and the internal pressure $p \in M_h$ such that (4.5–4.8) hold for all $(\tilde{\mathbf{u}}, \tilde{\mathbf{S}}, \tilde{\mathbf{F}}_e, \tilde{p}) \in [V_h]^d \times [W_h]^{d^2} \times [W_h]^{d^2} \times M_h$. Remember that this scheme corresponds to the discontinuous Galerkin's method. The question of the choice of the weight spaces W_h for the approximation of the stress $\mathbf{S}$ and deformation gradient $\mathbf{F}$ is discussed in subsection 4.2.2.

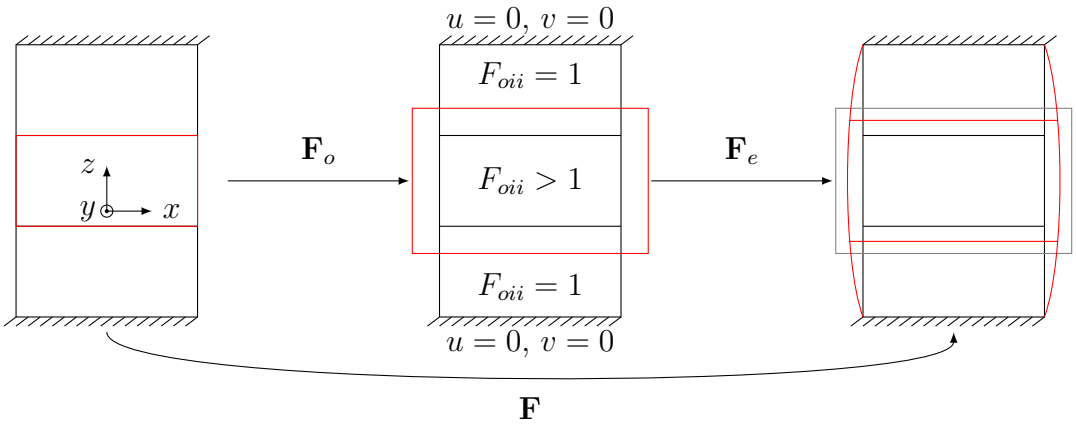

Figure 4.1: Distortion of the central part: $F_{oii} > 1$, $i = 1, 3$.

4.1.1 Example of a simple distortion

To reveal the important quantities to be observed the following simple example helps. For the sake of simplicity and the need not to loose the general aspects the two dimensional rectangular domain is considered as is sketched in figure 4.1 on the left. The central part is supposed to be distorted in the orthotropic way (Nardinocchi and Teresi, 2007)

$$\mathbf{F}_o = \alpha \mathbf{e}_1 \otimes \mathbf{e}_1 + \beta \mathbf{e}_2 \otimes \mathbf{e}_2 + \gamma \mathbf{e}_3 \otimes \mathbf{e}_3 \,, \tag{4.9}$$

with a positive α, β and γ, see the central part of figure 4.1. It is worth noting that when the fields are equal to one then $\mathbf{F}_o$ becomes identity $\mathbf{I}$ and no distortion occurs. A visible deformation is described by the gradient of placement $\mathbf{F}$ and due to compatibility conditions the object reaches the form of a deformed red body

as in figure 4.1 on the right. Therefore the displacement $\mathbf{u}$ and its gradient $\nabla\mathbf{u}$ has a form similar to the one included in figure 4.2 on the left (here has been sketched approximately the third component). It should be noted that in the axis directions the components of the displacement vector are defined

$$\mathbf{u} = (u, v, w)^{\mathrm{T}} = u\mathbf{c}_1 + v\mathbf{c}_2 + w\mathbf{c}_3 \,. \tag{4.10}$$

The determinants of the distortion, deformation and elastic deformation J_o, J and J_e are respectively sketched in figure 4.2 on the right.

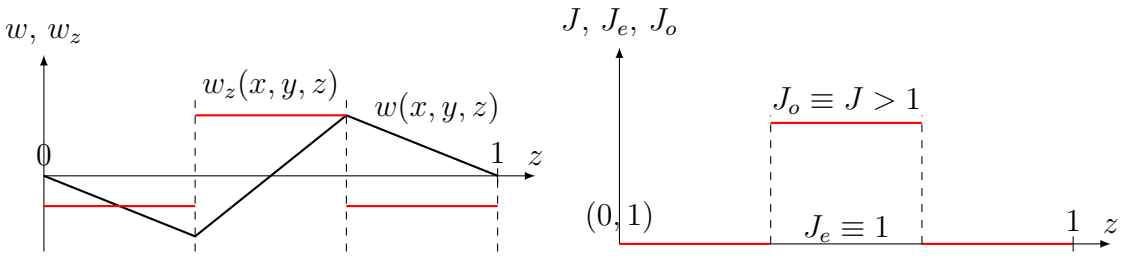

Figure 4.2: The displacement and its gradient on the left. The Jacobian of distortion, deformation and elastic deformation is on the right.

The displacement $\mathbf{u}$ and the Jacobian of elastic deformation J_e are continuous in the z direction and for this reason can be taken as the two kinematical reference quantities to be observed in numerical tests.

4.1.2 Numerical observation on the unit cube

A basic numerical test is performed on the isotropic unit cube. The introduced model contains a nearly incompressible neo-Hooke material. Instead of the theoretical behaviour of the problem described in the previous subsection it can be observed the above mentioned numerical oscillations near the zone where the step change of distortion occurs, see the illustration in figures 4.3 and 4.4.

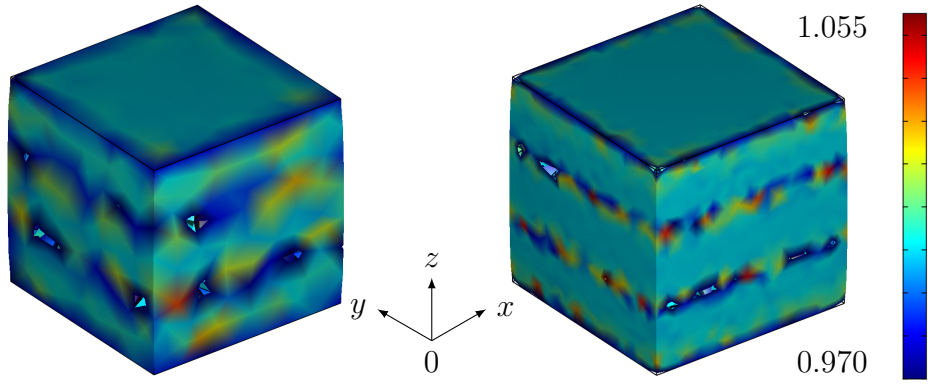

Figure 4.3: 3D example of Jacobian of elastic deformation J_e oscillations. On the left coarse mesh with 4816 elems and 23138 dof and the right the fine one with 40782 elems and 182600 dof.

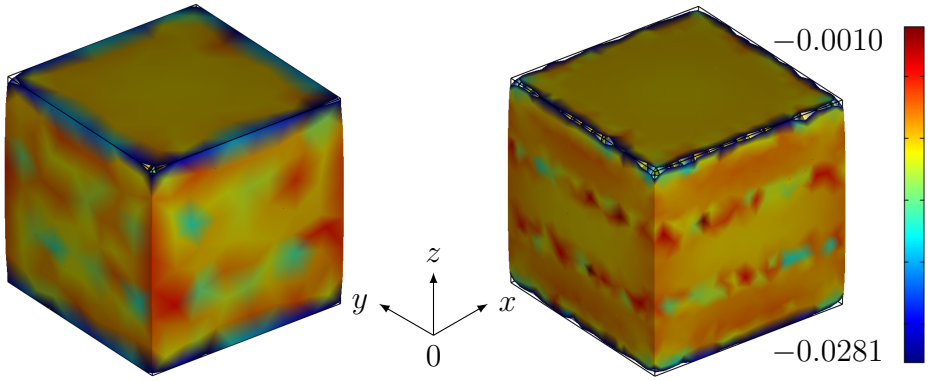

Figure 4.4: 3D example of oscillations of the first Piola–Kirchhoff component of stress S_{11}. On the left the coarse mesh with 4816 elems and 23138 dof and on the right the fine one with 40782 elems and 182600 dof.

The problem is set as sketched in figure 4.5. The boundary conditions on the faces parallel with yx-plane fix the displacement in all three directions (zero Dirichlet b.c. for u, v, w) and the rest of the boundary is without kinematical constraints. No external contact loads are applied, hence the zero Neumann boundary conditions are considered on the whole boundary. This can be summarized as follows

$$\begin{aligned} &\text{bottom and top basis fixed: } (u(x,y,a), v(x,y,a), w(x,y,a)) = (0,0,0)\,, \\ &xz\text{-plane parallel face free: } (u(x,a,z), v(x,a,z), w(x,a,z)) = (\cdot,\cdot,\cdot)\,, \\ &yz\text{-plane parallel face free: } (u(a,y,z), v(a,y,z), w(a,y,z)) = (\cdot,\cdot,\cdot)\,, \end{aligned} \tag{4.11}$$

with $a = 0$ or $a = 1$.

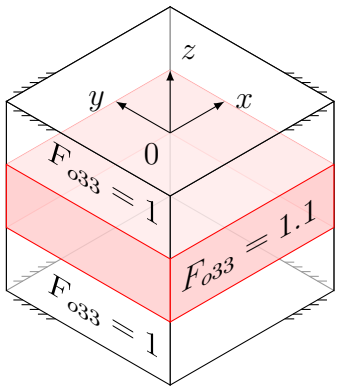

Figure 4.5: The unit cube is supposed to be distorted in the central part with $F_{o33} = 1.1$ while its bottom and top basis are constrained like in (4.11).

A significant example has been chosen to show the phenomena of oscillations where the dilatation can only take place in the direction perpendicular to the constrained faces. Hence the components of the distortion tensor are the following

$$|\mathbf{F}_o| = \begin{pmatrix} 1 & 0 & 0 \\ 0 & 1 & 0 \\ 0 & 0 & F_{o33} \end{pmatrix} \tag{4.12}$$

and as it is sketched in figure 4.5 the the way of action of dilatation F_{o33} is defined as the step function of the form

$$F_{o33} = \begin{cases} 1.1 \text{ for } 1/3 < z < 2/3 \\ 1 \text{ elsewhere}\,. \end{cases} \tag{4.13}$$

The bulk modulus κ is chosen as $\kappa = 10^4\mu$, see (Papoulia, 1995). The value of the shear modulus μ is 0.1. Either with the coarse or the fine mesh one

can observe the oscillations near the plane of distortion discontinuity. As it is demonstrated in subsection 4.1.1 this effect is only due to the computational procedure and has no physical meaning. It is worth noting that even if the finer mesh is used this cumbersome behaviour does not vanish. For any basic observation in three dimensions the high computational costs are to be faced. Therefore some simplified cases are to be analysed to hypothesise the reasons of such a behaviour and find some approach that improves the quality of the solution. Two basic significant examples are constructed: the plane strain and then the uniaxial strain problem.

4.2 The plane strain problem

The following two dimensional problem is taken directly from the illustrative example introduced in subsection 4.1.2. The configuration remains the same as it is sketched in figure 4.5 except that the with yz-plane parallel faces are blocked against the displacement in the direction of the x axis, which can be summed up as follows

$$\begin{aligned} &\text{bottom and top basis fixed: } (u(x,y,a), v(x,y,a), w(x,y,a)) = (0,0,0)\,, \\ &xz\text{-plane parallel face fixed: } (u(x,a,z), v(x,a,z), w(x,a,z)) = (\cdot,0,\cdot)\,, \\ &yz\text{-plane parallel face free: } (u(a,y,z), v(a,y,z), w(a,y,z)) = (\cdot,\cdot,\cdot)\,, \end{aligned} \tag{4.14}$$

where $a = 0$ or $a = 1$. The two dimensional plane strain problem is then obtained with the following domain illustrated in figure 4.6. The reason why the plane strain formulation has been chosen and not the plane stress one is because it is difficult to explicitly express the components of the deformation tensor $\mathbf{F}$ as a function of the components of the first Piola–Kirchhoff reference stress tensor $\mathbf{S}$. It is especially true when the nearly incompressible isotropic neo-Hookean material is used because then a lot of non linearities occur.

4.2.1 The plane strain problem formulation

Values of components of the deformation tensor $\mathbf{F}$ and of the distortion tensor $\mathbf{F}_o$ are introduced performed and their influence on the form of the first Piola–Kirchhoff reference stress tensor $\mathbf{S}$ is analysed. The planar deformations

within the chosen form of the distortion are described by the tensors as follows

$$|\mathbf{F}| = \begin{pmatrix} F_{11} & 0 & F_{13} \\ 0 & 1 & 0 \\ F_{31} & 0 & F_{33} \end{pmatrix}, \quad |\mathbf{F}_o| = \begin{pmatrix} F_{o11} & 0 & F_{o13} \\ 0 & F_{o22} & 0 \\ F_{o31} & 0 & F_{o33} \end{pmatrix}. \tag{4.15}$$

Here the distortion tensor also determines a dilatation or a contraction in the y-axis, which is the direction of the constrained deformation in the xz-plane. It should be noted that in the case of $F_{o22} = 1$, the pure planar distortions appear.

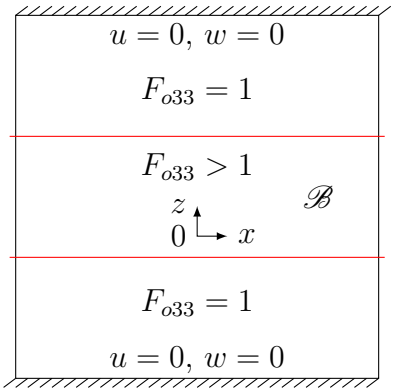

Figure 4.6: Two-dimensional body $\mathscr{B} = (0,1) \times (0,1)$ on which numerical tests are performed.

After the first Piola–Kirchhoff reference stress tensor $\mathbf{S}$ has been expressed in function of the deformation $\mathbf{F}$ and of the distortion $\mathbf{F}_o$ as given in (4.15), $\mathbf{S}$ becomes

$$|\mathbf{S}| = \begin{pmatrix} S_{11} & 0 & S_{13} \\ 0 & S_{22} & 0 \\ S_{21} & 0 & S_{33} \end{pmatrix}, \tag{4.16}$$

where the usually non zero component S_{22} depends on F_{ij}, F_{oij}, $i, j \in \{1, 3\}$ and on F_{o22} in the following manner

$$S_{22} = \mu J_e^{-\frac{2}{3}} (1 - \frac{1}{3} I_{e1} F_{o22}^2) \frac{J_o}{F_{o22}^2} - p J_e \,. \tag{4.17}$$

In respect of the balance (2.32) the component S_{22} should be a general function in the xz-plane only and the derivative in the direction of the y-axis should

vanish. Therefore the necessary and sufficient condition that $S_{22} = S_{22}(x, z)$ and $S_{22}(y) \equiv const.$ is valid if and only if $F_{o22} = F_{o22}(x, z)$ and $F_{o22}(y) \equiv const.$ Leaving the three dimensional frame to work on the plane strain problem, the unknown quantities become $\mathbf{u} = (u, w)$ for the displacement, p for the internal pressure, F_{eij}, $i, j \in \{1, 2\}$ for the elastic deformation tensor and S_{ij}, $i, j \in \{1, 3\}$.

4.2.2 Numerical observations in the plane strain problem

Several numerical tests on the square domain are performed. The mixed method (4.1–4.2) and the dVHW numerical scheme (4.5–4.8) for the nearly incompressible, isotropic, neo-Hookean material are implemented. The benchmark problem is described by the balance (2.32) where the internal force $\mathbf{d} = \mathbf{0}$ and the external forces $\mathbf{c} = \mathbf{0}$ and where the boundary conditions (4.14) are as sketched in figure 4.6. Because of the high non linearity of the problem, the COMSOL Multiphysics PDE Mode toolbox (COM, 2008) has been used as a finite element implementation. The necessity of a better control of the mesh quality leaded to the choice of the GMSH mesh generator (Geuzaine and Remacle, 2009, 2010).

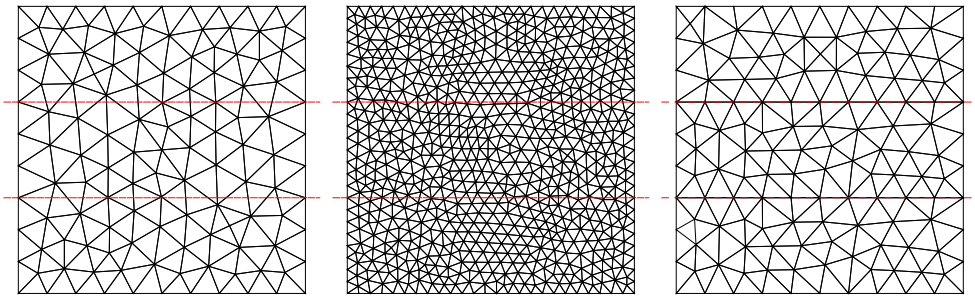

Figure 4.7: From left to right: the "coarser", "finer" and "partitioned" mesh with respectively 206, 1382 and 236 triangular elements.

The meshes which were created by GMSH and consequently loaded by COMSOL for the numerical computations are sketched in figure 4.7. The meshes construction is described in Appendix B. The analysis of the oscillations of the quantity of the stress component S_{33} and of the determinant of the elastic deformation J_e has been performed near the zones of discontinuity as they are sketched by parallel red lines in figures 4.7. Regarding the influence on the quality of the so-

lution three main principal case directions have been selected. At the beginning different kinds of elements have been applied and then the results compared. After that the mesh fineness and the arrangement of the elements edges have been tested along the red line. In all the figures 4.8–4.13 the limits for the Jacobian of elastic deformation are $J_e \in \langle 0.97, 1.055 \rangle$ and for the stress component $S_{33} \in \langle -0.0281, -0.001 \rangle$. The value of the shear modulus μ is 0.1 again and the bulk modulus related with it is $\kappa = 10^4 \mu$.

The discussion about the element types:
Tests with the first and second order Lagrange and discontinuous elements ave been performed for the stress $\mathbf{S}$ and the elastic deformation $\mathbf{F}_e$ in relations (4.6) and (4.7) following the dVHW method (4.5–4.8). The results for J_e and S_{33} are illustrated in figures 4.8 and 4.9. When the first order Lagrange elements Lag_1 were used the system matrix was singular. The convergence was achieved only when using the Lag_2 elements. However the oscillations of the solution can be observed near the discontinuity zones, see figures 4.8 and 4.9 on the right. It is worth noting that after the interpolation was performed the spreading of oscillations could be observed over the whole domain.

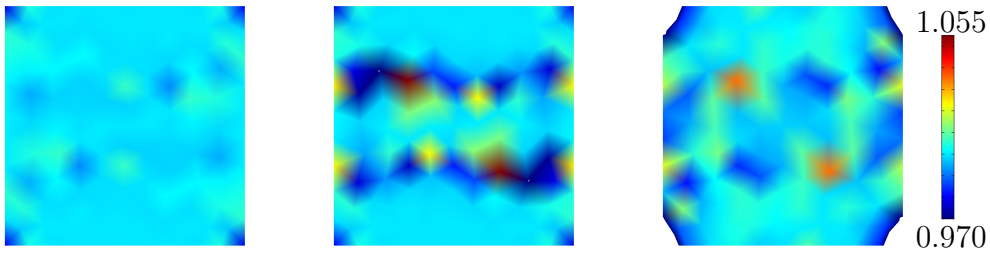

Figure 4.8: The Jacobian of the elastic deformation J_e on the "coarser" mesh with a choice of different kinds of elements for the first Piola–Kirchhoff stress $\mathbf{S}$ and the elastic deformation $\mathbf{F}_e$ in (4.6–4.7) as from left to right: Dsc_1, Dsc_2, Lag_2.

The quadratic Lagrange and discontinuous elements Lag_2 and Dsc_2 generally give higher oscillations than the first order discontinuous elements Dsc_1, see figures 4.8 and 4.9. It is therefore reasonable to use the first order discontinuous elements for $\mathbf{S}$ and $\mathbf{F}_e$.

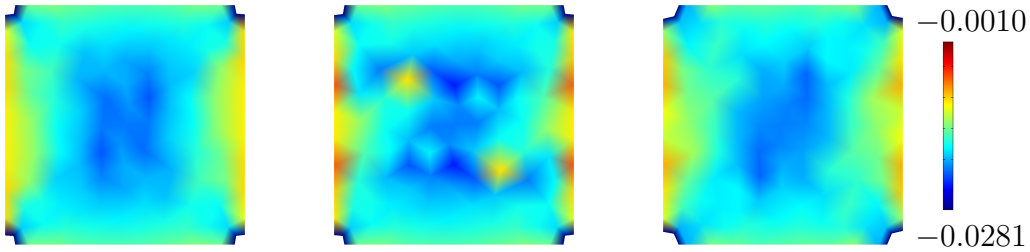

Figure 4.9: The component of the first Piola–Kirchhoff stress tensor S_{33} on the "coarser" mesh with a choice of different kinds of elements for the stress $\mathbf{S}$ and the elastic deformation $\mathbf{F}_e$ in (4.6–4.7) as from left to right: Dsc_1, Dsc_2, Lag_2.

The use of discontinuous elements Dsc for the stress $\mathbf{S}$ and the deformation $\mathbf{F}$ results more appropriate considering the relation in (Johnson, 2009)

$$V_h \subset H^1(\mathscr{B}) \Leftrightarrow V_h \subset C^0(\bar{\mathscr{B}})\,. \tag{4.18}$$

This relation could explain the cumbersome behaviour when the Lagrange elements Lag are used.

From now on the first order discontinuous elements Dsc_1 are used for the dependent variables of the first Piola–Kirchhoff stress $\mathbf{S}$ and the elastic deformation $\mathbf{F}_e$ following the proper methods, see table 4.1.

method\variable	**u**	p	**S**	$\mathbf{F}_e$
Mixed	Lag_2	Lag_1	–	–
dVHW	Lag_2	Lag_1	Dsc_1	Dsc_1

Table 4.1: Elements for proper variables in the mixed and dVHW method.

The discussion about the mesh fineness:
The other important observation is that the solution behaviour according to the mesh refinement. The first "coarser" and the second "finer" mesh were used from figure 4.7. The tests results following the mixed and dVHW method with the elements from table 4.1 are illustrated in figures 4.10 and 4.11.

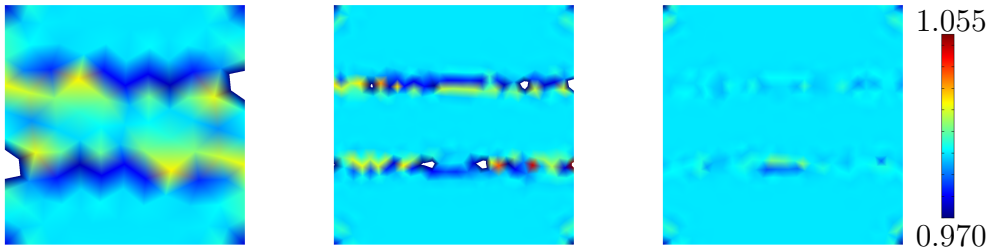

Figure 4.10: The Jacobian of the elastic deformation J_e with elements chosen according to table 4.1 as from left to right: the mixed method on "coarser" mesh, the mixed method on "finer" mesh, the dVHW scheme on "finer" mesh.

When the "finer" mesh is used the oscillations do not vanish neither for the mixed nor for the dVHW method. But using the dVHW scheme the solution quality has improved anyway, see figures 4.10 and 4.11.

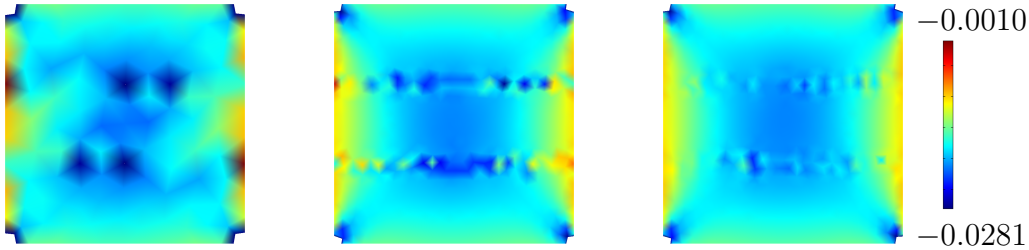

Figure 4.11: The component of the first Piola–Kirchhoff stress tensor S_{22} with elements chosen according to table 4.1 as from left to right: the mixed method on "coarser" mesh, the mixed method on the "finer" mesh, the dVHW scheme on "finer" mesh.

The discussion about the mesh arrangement:
The tests have been performed on the first "coarser" and the third "partitioned" mesh from figure 4.7. The right one contains the elements whose edges coincide with the red zone of distortion discontinuity. As one can see see from figures 4.12 and 4.13 the oscillations have not vanished for the meshes that does respect the discontinuity. Even while following the dVHW scheme, the solution near the boundary reaches unexpected values. It should be noted that there is no improvement using the mixed method on the "partitioned" mesh rather than on the "coarser" one, see figures 4.10–4.13.

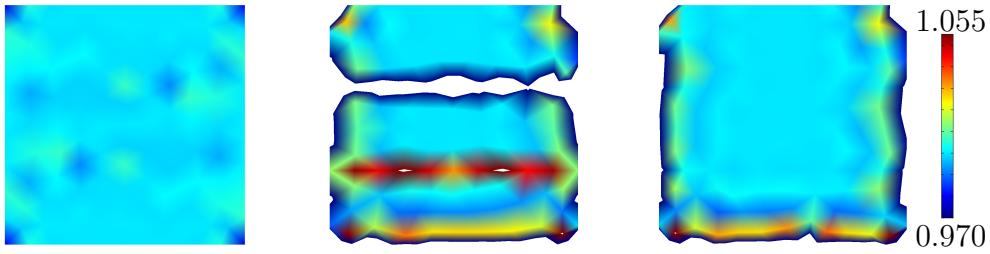

Figure 4.12: The Jacobian J_e of the elastic deformation $\mathbf{F}_e$ with elements used as in table 4.1 as from left to right: the dVHW method on the "coarser" mesh the mixed method on the "partitioned" mesh and the dVHW scheme on "partitioned" mesh.

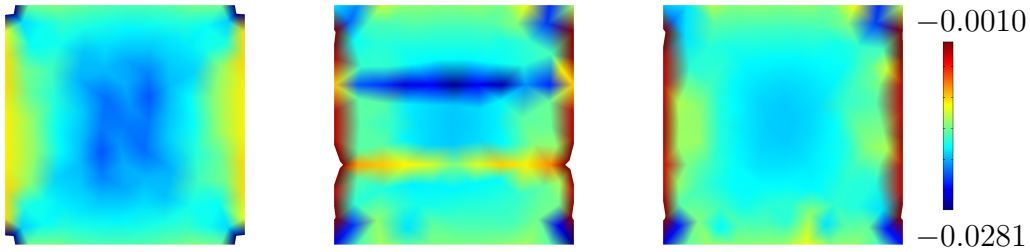

Figure 4.13: The component of the first Piola–Kirchhoff stress tensor S_{22} with elements used as in table 4.1 as from left to right: the dVHW method on "coarser" mesh, the mixed method on the "partitioned" mesh and the dVHW scheme on "partitioned" mesh.

According to the chosen discontinuous elements Dsc_1 for the approximation of the deformation gradient $\mathbf{F}$ and the stress $\mathbf{S}$ in the dVHW formulation the computation already gives good results on the coarse mesh. The numerical tests demonstrate that the mesh refinement yields better results than its geometrical adaptation in the zones of discontinuities.

4.3 The uniaxial strain problem

For a more exact description of the numerical solution quality it is useful to introduce a simplified problem which has got an exact solution. Like in the previous section the isotropic nearly incompressible neo-Hooke material model

is used. The balance (3.15) in the classical form is to be satisfied on the reference configuration. Therefore the first Piola–Kirchhoff reference stress is

$$\mathbf{S} = \mu J_o^{\frac{5}{3}} J^{-\frac{2}{3}} (\mathbf{F}\mathbf{C}_o^{-1} - \frac{1}{3}(\mathbf{C} \cdot \mathbf{C}_o^{-1})\mathbf{F}^{-\mathrm{T}}) - pJ\mathbf{F}^{-\mathrm{T}}\,, \quad p = -\kappa(J/Jo - 1)\,, \tag{4.19}$$

with κ as a bulk modulus.

4.3.1 Problem formulation in 3D and 1D

The three dimensional problem formulation which under certain conditions can lead to its the one dimensional version is sketched in figure 4.14. Neither external contact forces nor bulk loads are considered.

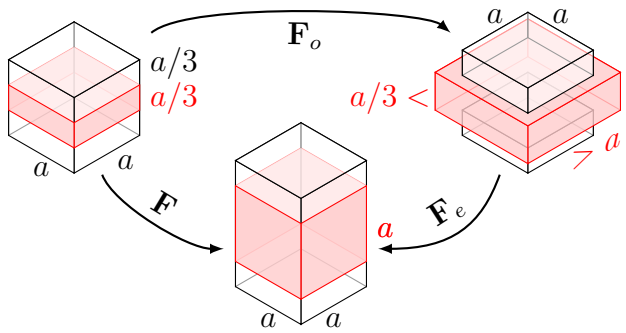

Figure 4.14: The three dimensional problem example with a distortion discontinuity illustrated on the cube whose height is a. Perpendicular edges of the base are identified with x and y axis and the vertical one from bottom to top with oriented z axis.

Only the central part is supposed to be distorted by $\mathbf{F}_o$ while applying certain kinematic boundary conditions. The bottom basis is fixed against any displacement in all directions and the lateral faces are free except for the constraint in the direction of the outwards boundary normal vector $\mathbf{n}$. The boundary conditions can be summed up as follows

$$\begin{aligned}
\text{bottom basis fixed: } & (u(x,y,0), v(x,y,0), w(x,y,0)) = (0,0,0)\,,\\
\text{top basis free: } & (u(x,y,1), v(x,y,1), w(x,y,1)) = (\cdot,\cdot,\cdot)\,,\\
xz\text{-plane parallel face: } & (u(x,a,z), v(x,a,z), w(x,a,z)) = (\cdot,0,\cdot)\,,\\
yz\text{-plane parallel face: } & (u(a,y,z), v(a,y,z), w(a,y,z)) = (0,\cdot,\cdot)\,,
\end{aligned} \tag{4.20}$$

with $a = 0$ or $a = 1$. The distortion tensor $\mathbf{F}_o$ will be in a special form that only admits the dilatation or contraction in the direction of the three main axes x, y and z, see (4.21). The problem set on the domain $\mathscr{B}$ in figure 4.14 with the already defined distortion $\mathbf{F}_o$ consists in finding a displacement field $\mathbf{u}$ so that the balance (2.33) and the boundary conditions (4.20) are satisfied with $\mathbf{d} \equiv \mathbf{0}$ and $\mathbf{c} \equiv \mathbf{0}$. To make a problem simpler, it is possible to expand the zone of distortion to the whole domain $\mathscr{B}$ as it is sketched in figure 4.15. When the analytical solution is found, then its generalization to the original problem is easy to be found.

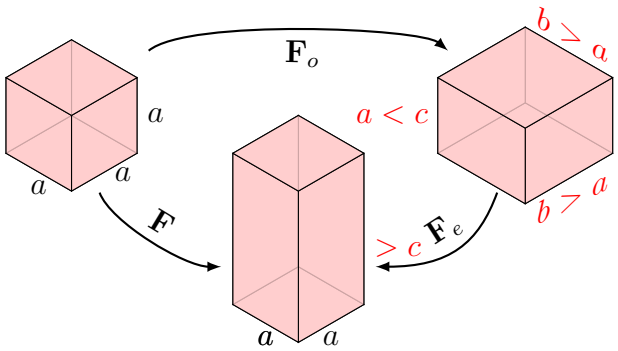

Figure 4.15: The three dimensional problem example with with the zone of distortion discontinuity expanded to the whole domain which is the cube of size a. Axes are defined as in figure 4.14.

Regarding the boundary conditions (4.20) and the form of the distortion tensor

$$\mathbf{F}_o = F_{oii}\mathbf{e}_i \otimes \mathbf{e}_i \,, \tag{4.21}$$

the following hypothesis can be introduced on the problem kinematics. The displacement field is

$$|\mathbf{u}| = \begin{pmatrix} 0 \\ 0 \\ w(z) \end{pmatrix} \,, \quad \text{hence} \quad |\mathbf{F}| = \begin{pmatrix} 1 & 0 & 0 \\ 0 & 1 & 0 \\ 0 & 0 & F_{33} \end{pmatrix} \,, \tag{4.22}$$

where F_{33} is only a general function of z, i.e. $F_{33}(z)$ only. Therefore all the components of the first Piola–Kirchhoff reference stress $\mathbf{S}$ depends on z only. Es-

pecially $S_{11}(x, y, \cdot)$ and $S_{22}(x, y, \cdot)$ are constant in x, y variables and the reference balance (2.33) with $S_{11'1} = 0$ and $S_{22'2} = 0$ holds automatically. The one dimensional problem can be set looking for a displacement $w(z)$ that holds the balance on the reference domain $\mathscr{B} = (0, 1)$ as follows with, the here under, boundary conditions:

$$\text{with} \quad S'_{33} = 0\,, \qquad \text{for } z \in (0,1)\,, \quad \text{BC: } w(0) = 0 \text{ and } S_{33}|_{z=1} = s = 0\,, \tag{4.23}$$

where the prime denotes the derivative in z.

4.3.2 The exact solution of the 1D problem

When the distortion (4.21) is considered and the derivative of the stress component S_{33} in $(4.19)_1$ is written in detail then it holds

$$S'_{33} = F'_{33}(\frac{2}{9}\mu J_o^{\frac{5}{3}} F_{o33}^{-2} F_{33}^{-\frac{2}{3}} + \frac{5}{9}\mu J_o^{\frac{5}{3}}(F_{o11}^{-2} + F_{o22}^{-2})F_{33}^{-\frac{8}{3}} + \kappa J_o^{-1}) = 0\,, \tag{4.24}$$

from which follows that a general real solution for the displacement is

$$w(z) = c_1 z + c_2\,, \tag{4.25}$$

where c_1 and c_2 are real constants. From the first boundary condition $(4.23)_2$ it is possible to deduct $c_2 = 0$. The constant c_1 can be obtained from the last boundary condition in $(4.23)_3$, which means solving the following equation

$$S_{33} = \frac{\mu}{3} J_o^{\frac{5}{3}} F_{o33}^{-2} F_{33}^{\frac{1}{3}}(2 - F_{o33}^{-2}(F_{o11}^{-2} + F_{o22}^{-2})F_{33}^{-2}) + \kappa(F_{33}J_o^{-1} - 1) = 0\,, \tag{4.26}$$

where the unknown constant c_2 is embedded in the root F_{33}. Due to the presence of rational exponents some problems occur while looking for the solution. Anyway it is possible to find a solution only if all coefficients are given numbers.

The displacement $w(z) = (0.21)z$[m], when $F_{o11} = F_{o22} = 1.1$[1], ($\mu = 0.1$[Pa], $\kappa = 10^5$[Pa]).

Other results are: $p = -\frac{1}{3}\mathrm{tr}\,\mathbf{T} = 0.0425104$[Pa], $S_{11} = S_{22} = -0.0771563$[Pa]. Therefore as far as the displacement is concerned, the kinematical equation holds

$$w(z) = (J_o - 1)z\,. \tag{4.27}$$

However such relation can be directly obtained only using the purely incompressible approach and does not satisfy relation (4.26). Therefore the displacement is introduced in the following form

$$w(z) = (1-\varepsilon)(J_o - 1)z\,, \quad \varepsilon > 0\,. \tag{4.28}$$

The condition (4.26) then becomes as follows

$$S_{33} = \frac{\mu}{3} J_o^{\frac{5}{3}} F_{o33}^{-2}(J_o - \varepsilon(J_o-1))^{\frac{1}{3}}(2 - F_{o33}^{-2}(F_{o11}^{-2} + F_{o22}^{-2})(J_o - \varepsilon(J_o-1))^{-2}) - p = 0\,, \tag{4.29}$$

with the internal pressure

$$p = -\kappa\varepsilon\frac{1-J_o}{J_o}\,, \tag{4.30}$$

which reaches a finite value $|p| < \infty$. From this can be deduced that ε is a function of κ as $\varepsilon = \varepsilon(\kappa)$ satisfying

$$\varepsilon \xrightarrow[\kappa\to\infty]{} 0\,, \quad \text{and} \quad \frac{1}{\varepsilon} = O(\kappa)\,. \tag{4.31}$$

This gives physically the reasonable property of the internal pressure in function of the distortion

$$\begin{array}{l} F_{o11} < 1 \text{ and } F_{o22} < 1 \\ F_{o11} > 1 \text{ and } F_{o22} > 1 \end{array} \Rightarrow \begin{array}{l} p < 0 \\ p > 0 \end{array}. \tag{4.32}$$

The obtained information about the solution of problem (4.23) is sufficient to determine the computational error.

All these results can also be obtained numerically on the cube in three-dimensional frame. The tests performed by COMSOL provide the same values and response as those obtained from the one dimensional problem.

When the distribution of the distortion in the body, as in figure 4.14, takes

the form

$$F_{o11}(z) = F_{o22}(z) = \begin{cases} 1.1 \text{ for } 1/3 < z < 2/3 \\ 1 \qquad \text{otherwise} \end{cases} \quad \text{and} \quad F_{o33} \equiv 1\,, \quad z \in (0,1)\,, \tag{4.33}$$

then the effect in the displacement $w(z)$, in the determinant of deformation gradient J and in the stress

$$S_{ii} = \mu J_o^{\frac{5}{3}} F_{33}(F_{oii}^{-2} - \frac{1}{3}(F_{33}^2 F_{o33}^{-2} + F_{o11}^{-2} + F_{o22}^{-2})) + \kappa(F_{33}/J_o - 1)F_{33} \quad i = 1,2\,, \tag{4.34}$$

is sketched in figure 4.16.

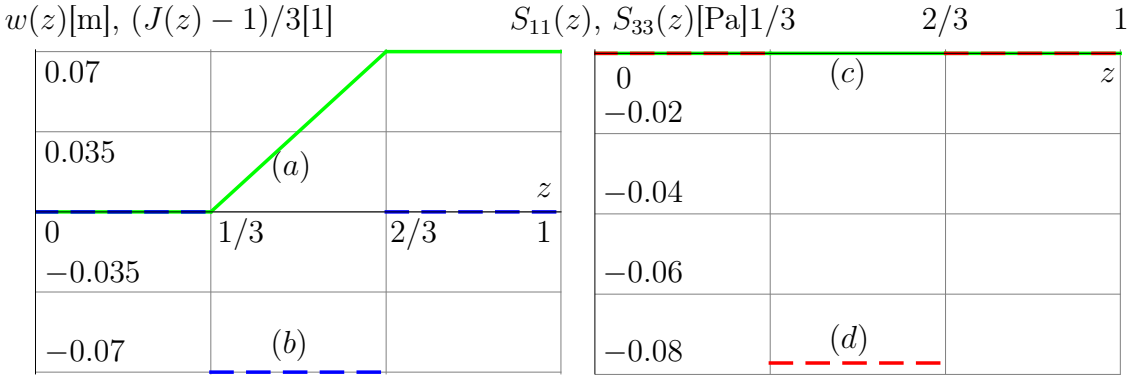

Figure 4.16: The solution of the one dimensional problem with the distortion discontinuities from (4.33). On the left there are the green solid line (a), the displacement $w(z)$, the blue dashed line (b), the scaled Jacobian of elastic deformation $(J(z) - 1)/3$ and on the right, there are the green solid line (c), the stress $S_{33}(z)$, the red dashed line (d) and the stress $S_{11} = S_{22}$.

4.3.3 The formulation of the one dimensional schemes

In order to proceed with the analysis of the mixed and dVHW methods behaviour the numerical schemes must be constructed following the simplified example from figure 4.14 described by balance (4.23).

The compatible formulation:

The problem (4.23) expressed in the classic form can be reformulated in the weak

form in the one dimensional reference domain as follows

$$0 = \int_0^1 S'_{33}(w(z))\tilde{w}(z)\,dz = [S_{33}(w(z))\tilde{w}(z)]_0^1 - \int_0^1 S_{33}(w(z))\tilde{w}'(z)\,dz = \\ = s\tilde{w}(1) - \int_0^1 S_{33}(w(z))\tilde{w}'(z)\,dz\,. \tag{4.35}$$

Hence for $s = 0$ holds

$$-\int_0^1 S_{33}(w)\tilde{w}'\,dz = 0\,, \quad \text{for all } \tilde{w} \in H_0^1(0,1)\,. \tag{4.36}$$

In a computational context the numerical scheme (4.36) corresponds to the variational formulation of the compatible method (3.16). It should be noted that the form on the left side of balance (4.36) is neither symmetric nor linear in w.

The mixed displacement–pressure formulation:

When the stress component $S_{33}(z) = S_{33}(w(z), p(z))$ depends on both the displacement $w(z)$ and internal pressure $p(z)$, the mixed formulation in the reference domain $z \in (0,1)$ corresponding to (4.1–4.2) is

$$\int_0^1 -S_{33}(w,p)\tilde{w}'\,dz + [S_{33}(w)\tilde{w}]_0^1 = 0\,, \quad \text{for all } \tilde{w} \in H_0^1(0,1)\,, \tag{4.37}$$

$$\int_0^1 (\frac{p}{\kappa} + J_o^{-1}(1+w') - 1)\tilde{p}\,dz = 0\,, \quad \text{for all } \tilde{p} \in L^2(0,1)\,. \tag{4.38}$$

In the weak balance (4.8) (incompressibility) for the volumetric distortion (4.21) and for the spherical part of the deformation energy (2.57) it has been used the following form of the elastic deformation tensor

$$|\mathbf{F}_e| = \begin{pmatrix} F_{o11}^{-1} & 0 & 0 \\ 0 & F_{o22}^{-1} & 0 \\ 0 & 0 & (1+w'(z))F_{o33}^{-1} \end{pmatrix}. \tag{4.39}$$

The de Veubeke–Hu–Washizu formulation:

In the de Veubeke–Hu–Washizu formulation (4.5–4.8) for the incompressible material the stress depends on the elastic deformation $\mathbf{F}_e = \mathbf{F}_e(\mathbf{F})$ and on the internal pressure $p = p(\mathbf{F})$. This leads to the dVHW formulation in one dimension as follows

$$\int_0^1 -S_{33}(F_{e33}, p)\tilde{w}'\,dz + [S_{33}(F_{e33}, p)\tilde{w}]_0^1 = 0\,, \quad \text{for all } \tilde{w} \in H_0^1(0,1)\,, \tag{4.40}$$

$$\int_0^1 (S_{33}(F_{e33}, p)F_{o33} - J_o S_{o33})\tilde{F}_{e33}\,dz = 0\,, \quad \text{for all } \tilde{F}_{e33} \in L^2(0,1)\,, \tag{4.41}$$

$$\int_0^1 (1 + w' - F_{e33}F_{o33})\tilde{S}_{33}\,dz = 0\,, \quad \text{for all } \tilde{S}_{33} \in L^2(0,1)\,, \tag{4.42}$$

$$\int_0^1 (\frac{p}{\kappa} + F_{e33}(F_{o11}F_{o22})^{-1} - 1)\tilde{p}\,dz = 0\,, \quad \text{for all } \tilde{p} \in L^2(0,1)\,, \tag{4.43}$$

where $S_{o33} = \left|\frac{\partial \psi_o}{\partial \mathbf{F}_e}\right|_{33}$. Hence

$$S_{o33} = \mu(F_{o11}F_{o22})^{\frac{2}{3}}F_{e33}^{-\frac{2}{3}}(F_{e33} - \frac{1}{3}(F_{o11}^{-2} + F_{o22}^{-2} + F_{e33}^{2})F_{e33}^{-1}) + \frac{\partial \psi_o}{\partial J_e}(F_{o11}F_{o22})^{-1}\,, \tag{4.44}$$

with $\frac{\partial \psi_o}{\partial J_e} = -p$ and the here under form of the elastic deformation tensor is applied

$$|\mathbf{F}_e| = \begin{pmatrix} F_{o11}^{-1} & 0 & 0 \\ 0 & F_{o22}^{-1} & 0 \\ 0 & 0 & F_{e33} \end{pmatrix}\,. \tag{4.45}$$

4.3.4 The numerical experiments

The numerical tests have been performed for the problem (4.23) with boundary conditions (4.20), see figure 4.14. All the scheme formulations have been used: the compatible one (4.36), the mixed one (4.37–4.38) and the dVHW method (4.40–4.43). The values for the distortion have been set as in (4.33) to reproduce the analytical solution like in subsection 4.3.2. First the numerical solution error has been found using the mixed and dVHW method. The displacement $w(z)$, the Jacobian J_e of the elastic deformation and the stress S_{ii}, $i = 1$ or $i = 2$ have been confronted. When the compatible and the mixed method were used then

the stress component resulted to be

$$S_{ii} = \mu J_o^{\frac{5}{3}} F_{33}^{-\frac{2}{3}} (F_{oii}^{-2} - \frac{1}{3}(F_{33}^2 F_{o33}^{-2} + F_{o11}^{-2} + F_{o22}^{-2})) - pF_{33}\,, \tag{4.46}$$

where $i = 1, 2$ (there is no summation over the index i) for the mixed method and $p = -\kappa(F_{33}/J_o - 1)$ for the compatible method. From the results obtained using the dVHW scheme the stress component was determined as resulted to be

$$S_{ii} = \mu J_o^{\frac{2}{3}} F_{oii}^{-1} F_{ojj} F_{o33}^{\frac{1}{3}} F_{e33}^{-\frac{2}{3}} (1 - \frac{1}{3} F_{oii}^2 (F_{e33}^2 + F_{o11}^{-2} + F_{o22}^{-2})) - pF_{o33}F_{e33}\,, \tag{4.47}$$

where $i = 1, 2$ and j depends on i as follows: $j = 2$ when $i = 1$ and $j = 1$ when $i = 2$. The errors ϵ in the energetic norm have been introduced as follows

$$\epsilon_w = \|w - w_h\|_{H_0^1(\mathscr{B})}\,, \quad \epsilon_{J_e} = \|J_e - J_{e_h}\|_{L^2(\mathscr{B})}\,, \quad \epsilon_{S_{22}} = \|S_{22} - S_{22_h}\|_{L^2(\mathscr{B})}\,. \tag{4.48}$$

The elements in the proposed methods have been used as it is listed in table 4.2.

method\variable	w	p	S_{33}	F_{e33}
Compatible	Lag_2	–	–	–
Mixed	Lag_2	Lag_1	–	–
dVHW	Lag_2	Lag_1	Dsc_1	Dsc_1

Table 4.2: Used elements in one dimensional schemes.

An equidistant discretization has been used for the domain $\mathscr{B} \equiv (0, 1)$. The errors in figures 4.17–4.18 are expressed in function of the number of elements present in the mesh which vary from 3 to 30. It is worth noting that the mixed method has provided the same results for the one dimensional problem as the dVHW scheme. Therefore only the errors of the compatible and dVHW methods are compared.

method\error	$\epsilon_w(n > 15)$	$\min\limits_{3<n<30} \epsilon_w$	$\epsilon_{J_e}(n > 15)$	$\epsilon_{S_{22}}(n > 15)$
Compatible	$\approx 10^{-4}$	$\approx 10^{-6}$	$\approx 10^{-1}$	$\approx 10^{2}$
dVHW	$\approx 10^{-3}$	$\approx 10^{-4}$	$\approx 10^{-1}$	$\approx 10^{-2}$

Table 4.3: The comparision between the error of the compatible and the dVHW method.

In figures 4.17–4.18 one can see for both methods that for the elements number $n = 3k$, $k = 1, 2, \ldots$ the error of displacement w reaches the local minima. The comparison of the errors between the compatible and the dVHW method are summarized in table 4.3. It is true that the displacement error ϵ_w is one order higher using the dVHW than using the compatible method, but the error regarding the determinant J_e of the elastic deformation is not worse with the dVHW method. And as far as the stress S_{22} is concerned, the error is even four order lower for the dVHW method than for the compatible one.

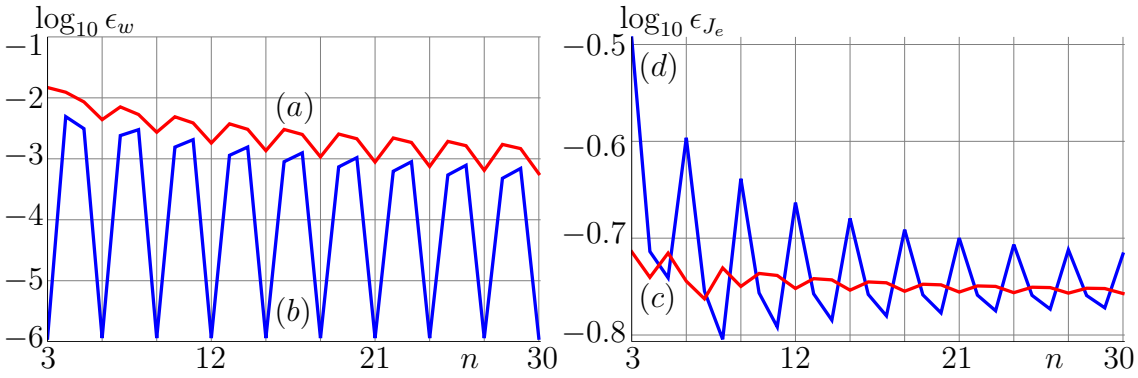

Figure 4.17: The computational error vs the number of elements n. On the left: the error of the displacement $w(z)$, on the right: error of Jacobian J_e of elastic deformation. For both figures: in red the dVHW method line (a), in blue the compatible scheme line (b).

It should be noted that for both methods when the error reaches the local minima for the displacement then the local maxima can be observed as far as the other quantities J_e and S_{22} are concerned. This happens when the elements number $n = 3k$, $k = 1, 2, \ldots$

As a consequence of the above observations and the fact that the same results

have been obtained for both the mixed and the dVHW method in one dimension, the following hypothesis can be stated for a two and three dimensional frame.

Hypothesis 1. In problems involving the nearly incompressible neo-Hookean isotropic material, described through the nonlinear elasticity characterized by large deformations and discontinuous distortions, and treated in a two or three dimensional manifold, the computational error in the kinematical quantities (like the displacement $\mathbf{u}$, or the Jacobian J_e) is bigger using the dVHW method than the mixed method, but is not bigger and even lower as far as the dynamic quantities like the stress $\mathbf{S}$ are concerned.

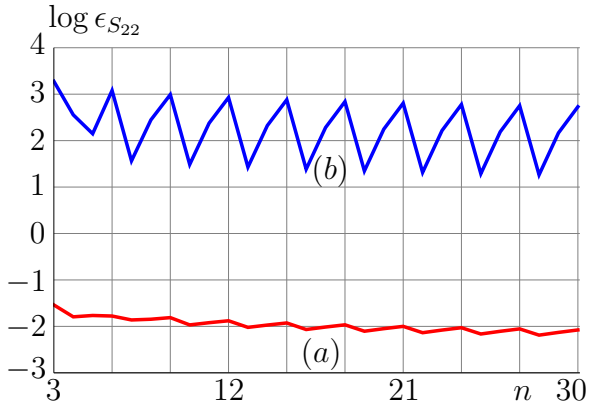

Figure 4.18: The computational error of the stress S_{22} vs the elements number n. In red the dVHW method line (a), in blue the compatible scheme line (b).

Chapter 5

Conclusion

To conclude the rigorous state exam in Pilsen on 16$^{\text{th}}$ June 2010, several possibilities were suggested including;

- Verify whether the oscillations depend on the form of the volumetric strain energy;
- Extend the problem to the three dimensions;
- Enrich the homogeneous material by the preferred property direction (anisotropy);
- Simplify the benchmark example in order to obtain an exact solution and observe the numerical error.

The forms of volumetric energy from (Hartmann and Neff, 2006) were implemented and the tests given the same oscillating solution for the mixed method as the volumetric energy (2.57) proposed in chapter 2. It should be noted that when the perturbed Lagrange multiplier mixed method (Simo and Taylor, 1991; Wriggers, 2008) and mixed method as outlined in (3.22–3.23) were used, then no difference on the solution was observed.

An extension to three dimensions was performed; however, in order to analyse the problem, the two-dimensional plain strain formulation, which in terms of degrees of freedom is much small than the three dimensional one, is sufficient. Even though the dVHW formulation can be reduced by the weak stress term, the full dVHW formulation (4.5–4.8) was prefered. This idea was based on the fact that for anisotropic materials, both the full dVHW and its reduced version

yield different results, but in the isotropic case, there are no differences. This highlights another issue for the anisotropic materials; i.e. the verification of the numerical solution obtained by the dVHW or its reduced version. The numerical results from the solution obtained by the reduced dVHW method and the mixed method are the identical. It is worth noting that the reduced dVHW formulation is, generally, more robust than the mixed method; moreover it avoids the locking effect, which appears particularly in the case of anisotropic materials. Although the above summary is beyond the scope of this thesis, it illustrates the main reasons for not considering the anisotropy; however applying anisotropy to the constitutive law should be an area for further study. This could be explored by using adaptive numerical methods.

The analytical results for computational error in chapter 4, show that the dVHW method behaves better than the mixed method in the most of problem configurations, similar to those described in chapter 4, especially in terms of the quantities of stress, see figure 4.18.

From the numerical tests on the two dimensional benchmark it was concluded that the first order discontinuous elements for the elastic deformation and the first Kirchhoff–Piola stress is the best choice. The coarse mesh provides satisfactory results. When the computation on the finer mesh is performed good results are obtained and it follows that the geometrical adaptation should be the subject of future research.

One of the advantages of the dVHW approach, is its ability to damp the oscillations near the zones of discontinuity. The disadvantage of this is the computational cost of the solved problem due to the number of degrees of freedom, which in three dimensional calculations is extremely high. The other possible issue to consider in this problem, is the suitability of the combined approaches: i.e. *hp*-FEM adaptivity (Šolín et al., 2003); isogeometric finite elements (Hughes et al., 2005); stabilization technique based on using of bubble functions (Codina, 1998; Franca and Farhat, 1995); or domain decomposition (Smith et al., 1996).

The application of the combined approach of implemented isogeometric FE and domain decomposition method is described in works (Daněk and Kutáková,

2008). This method of research can only be used for cases with a well defined position of zone of the discontinuity in the analysed manifold and for isotropic materials only. When the material with preferred stiffened direction is considered, the combined approach is not appropriate. The most suitable way to analyse general problems is therefore *hp*-FEM adaptivity, which automatically follows steep gradient zones. The preliminary research including the usage of the *hp*-FEM adaptivity can be described as follows

- To solve the 2D problem with the compatible formulation.
- When the compatible formulation does not converge, then use the mixed method.
- To apply the dVHW formulation and compare the results with the compatible/mixed approach.

Some possible generalization of my results are:

- The derived dVHW scheme is also suitable to be applied to all hyperelastic materials with distortions.
- It is applicable to the diffusion-convection-reaction problems.
- One-dimensional benchmark case can be formulated to more general cases, e.g. materials with exponential law for matrice or the anisotropic one.

Appendix A

Convention and integration rules

In the volume and surface integrals the differentials are automatically considered and for a practical reason are omitted in the text. The volumetric integrals in the reference and actual configuration are

$$\int_{\mathscr{P}\subset\mathscr{B}} (\cdot) := \int_{\mathscr{P}\subset\mathscr{B}} (\cdot)\, dV \quad \text{and} \quad \int_{\mathscr{P}_t\subset\mathscr{B}_t} (\cdot) := \int_{\mathscr{P}_t\subset\mathscr{B}_t} (\cdot)\, dv \tag{A.1}$$

and the surface integrals are

$$\int_{\partial\mathscr{P}\subset\partial\mathscr{B}} (\cdot) := \int_{\partial\mathscr{P}\subset\partial\mathscr{B}} (\cdot)\, dA \quad \text{and} \quad \int_{\partial\mathscr{P}_t\subset\partial\mathscr{B}_t} (\cdot) := \int_{\partial\mathscr{P}_t\subset\partial\mathscr{B}_t} (\cdot)\, da\,. \tag{A.2}$$

the derivative, used in *per partes* rule, on the reference and actual configuration is

$$\operatorname{Div}(\mathbf{A}^{\mathrm{T}}\mathbf{a}) = \operatorname{Div}\mathbf{A}\cdot\mathbf{a} + \mathbf{A}\cdot\nabla\mathbf{a}\,, \quad \operatorname{div}(\mathbf{A}^{\mathrm{T}}\mathbf{a}) = \operatorname{div}\mathbf{A}\cdot\mathbf{a} + \mathbf{A}\cdot\operatorname{grad}\mathbf{a}\,. \tag{A.3}$$

The Stokes identity on the reference and actual configuration is

$$\int_{\mathscr{B}} \operatorname{Div}\mathbf{a} = \int_{\partial\mathscr{B}} \mathbf{a}\cdot\mathbf{m}\,, \qquad \int_{\mathscr{B}_t} \operatorname{div}\mathbf{a} = \int_{\partial\mathscr{B}_t} \mathbf{a}\cdot\mathbf{n}\,. \tag{A.4}$$

Appendix A

Appendix B

Implementation to COMSOL

For the implementation with COMSOL Multiphysics 3.5a the *partial differential equation (PDE) modes* module was used for the equation-based modelling. In the illustration example the implementation of the problem of non linear elasticity is shown in a three dimensional frame using the nearly incompressibile isotropic neo-Hookean material. The numerical scheme is the mixed method (3.22–3.23) as it is mentioned in chapter 3.

First as far as the model explorer is concerned the problem dimension is to be chosen and then it is necessary to continue with *physics*. In order to define a *Time-dependent analysis* it is possible to choose from the *Application modes tree* the following option: *COMSOL Multiphysics*, *PDE Modes* and *Weak form Subdomain*. Every balance in the problem determines the proper *physics* and dependent variables, which can be called `u`, `v` and `w` for the displacement in the balance (3.22) in three dimensions and `p` for the pressure in the balance (3.23). Only the choice of the elements likely to change later remains.

The nonlinear elasticity:
At that point the computational domain is created, while the governing (balance) equations with BC and expressions containing the constitutive law is specified. The domain is defined in the `Draw` menu and the unitary cube (rectangle or line) is constructed with a corner at the origin. It is necessary to implement the mechanical balance (3.22) in the `Subdomain Settings` in which the following

physics is defined:

$$\int_{\mathscr{B}} \dot{\mathbf{u}} \cdot \tilde{\mathbf{u}} = \int_{\mathscr{B}} -\nabla \mathbf{u} \cdot \nabla \tilde{\mathbf{u}} + \int_{\mathscr{B}} \mathbf{d} \cdot \tilde{\mathbf{u}}\,, \tag{B.5}$$

where the displacement $\mathbf{u}$, test function $\tilde{\mathbf{u}}$ and their gradients $\nabla\mathbf{u}$, $\nabla\tilde{\mathbf{u}}$ have the following components

$$\mathbf{u} = \begin{pmatrix} \mathtt{u} \\ \mathtt{v} \\ \mathtt{w} \end{pmatrix}, \quad \nabla\mathbf{u} = \begin{pmatrix} \mathtt{ux}\ \mathtt{uy}\ \mathtt{uz} \\ \mathtt{vx}\ \mathtt{vy}\ \mathtt{vz} \\ \mathtt{wx}\ \mathtt{wy}\ \mathtt{wz} \end{pmatrix} \tag{B.6}$$

and

$$\tilde{\mathbf{u}} = \begin{pmatrix} \mathtt{test(u)} \\ \mathtt{test(v)} \\ \mathtt{test(w)} \end{pmatrix}, \quad \nabla\tilde{\mathbf{u}} = \begin{pmatrix} \mathtt{test(ux)}\ \mathtt{test(uy)}\ \mathtt{test(uz)} \\ \mathtt{test(vx)}\ \mathtt{test(vy)}\ \mathtt{test(vz)} \\ \mathtt{test(wx)}\ \mathtt{test(wy)}\ \mathtt{test(wz)} \end{pmatrix} \tag{B.7}$$

The "balance" (B.5) in COMSOL is schematically expressed as `dweak=weak`. In the case of elasticity the stationary problem is solved, therefore all the time derivative terms, the `dweak` ones, are automatically to be set to zero. Our goal is to implement the balance (3.22), thus the expressions in `Subdomain Settings` will be

`-S11*test(ux)-S12*test(uy)-S13*test(uz)+d1*test(u)`
`-S21*test(vx)-S22*test(vy)-S23*test(vz)+d2*test(v)`
`-S31*test(wx)-S32*test(wy)-S33*test(wz)+d3*test(w)`

Table B.1: Implementation of governing terms of "physics" – elasticity.

Because no bulk loads $\mathbf{d} = (d_1, d_2, d_3)^{\mathrm{T}}$ are considered everyone of its component `d1`, `d2` and `d3` is zero. Then every `dweak` term is set to zero and `Element` is chosen Lag_2 to every displacement components according to table B.2.

elem.	Lag_1	Lag_2	Dsc_1
impl.	`shlag(1,'fun')`	`shlag(2,'fun')`	`shdisc(3,1,'fun')`
int. ord.	2	4	2

Table B.2: An example of finite element specification in three dimensions for a dependent variable `fun`.

To fix the bottom and the top base of the cube in all directions it is automatically set in `Boundary Settings` every component row in `constr` equal to zero, thus it is sufficient to leave `-u`, `-v` and `-w` in the proper row. For every remaining choice of the faces zero is set everywhere.

Nearly incompressibility:
The following weak equation in the `Subdomain Settings` is inserted

```
(p/kappa+(Je-1))*test(p)
```

and the element in according to table B.2 has to be Lag_1 for the pressure `p`. It should be noted that in the case of the implementation of the dVHW method the elements for the stress components S_{ij} and the elastic deformation F_{eij} are defined as Dsc_1.

Boundary conditions are free in `constr` of `Subdomain settings`, thus zero for every face.

Variables and constants:
In the `Global variables` the values of every component of the first Piola–Kirchhoff stress tensor $\mathbf{S}$ are fixed according to the gradient of displacement $\nabla\mathbf{u}$. In the `Scalar variables` the input for the distortion is given by

```
Fo33=1+(dist-1)*(1/3<z)*(z<2/3)
```

In the `Constants` are fixed the material parameters `mu`, `kappa` and is defined the distortion `dist`.

Appendix B

Mesh

The optimized tetrahedral and triangular mesh generated by the Delaunay triangulation algorithm is used in the three and two dimensional domains. The mesh of the cube is set according to table B.3. For the two dimensional square domain the mesh loaded from GMSH generator is used and on the line for the simplicity the uniform mesh is used.

parameter	coarse mesh	finer mesh
max. el. scal. fact.	1.5	0.75
el. growth rate	1.6	1.45
mesh curv. fact.	0.7	0.5
mesh curv. cut.	0.04	0.02
resol. of narrow reg.	0.4	0.6

Table B.3: Mesh parameters for the cube.

When the GMSH generator is used in two dimensions, then the MeshAdapt algorithm is applied. An optimization was performed in order to try to decrease the number of 4-triangle nodes which lead to $\approx 90°$ angle between their sides. Then the mesh is carried to COMSOL through the `Mesh from file` menu and the new geometry based on the imported mesh is defined. Anyway because of missing documentation about the COMSOL mesh format this traffic is not direct and consists first in entering the mesh data into the `fem` structure and then in saving it in a file for a later elaboration.

Solver

The nonlinear and nonsymmetric problem is solved. In the `Stationary solver` the damped Newton method is used together with UMFPACK linear solver. The relative tolerance is equal to 10^{-6}.

Postprocessing

The element refinement is 1 and in the `Subdomain plot` the option `Coloring and fill` is set to be `Interpolated`.

Any further information about the implementation or the mesh format and the proper algorithm of its generation in GMSH can be to found in (COM, 2008; Geuzaine and Remacle, 2009, 2010).

Appendix B

References

D. Ambrosi and S. Pezzuto. Active stress vs. active strain in mechanobiology: Constitutive issues. *Journal of Elasticity*, 107:199–212, 2011. 19, 20

K.-J. Bathe. *Finite element procedures.* CPrentice Hall, Upper Saddle River, New Jersey, 1996. 2, 27

M.F. Beatty. Topics in finite elasticity: Hyperelasticity of rubber, elastomers, and biological tissues—with examples. *Applied Mechanics Reviews*, 40(12): 1699–1734, 1987. 13, 14, 15, 16

D. Braess. *Finite Elements: Theory, Fast Solvers, and Applications in Elasticity Theory.* Cambridge University Press, Cambridge, MA, 2007. 25, 28

S. C. Brenner and L. R. Scott. *The Mathematical Theory of Finite Element Methods.* Springer-Verlag, New York, 2007. 21

F. Brezzi and M. Fortin. *Mixed and Hybrid Finite Element Methods.* Springer-Verlag, New York, 1991. 27

C. Cherubini, S. Filippi, P. Nardinocchi, and L. Teresi. An electromechanical model of cardiac tissue: Constitutive issues and electrophysiological effects. *Progress in Biophysics and Molecular Biology*, 97(2–3):562–573, 2008. 1, 20

R. Cimrman and contributors. *SfePy Documentation, Release 2011.3*, August 2011. 3

R. Codina. Comparison of some finite element methods for solving the diffusion-convection-reaction equation. *Computer Methods in Applied Mechanics and Engineering*, 156:185–210, 1998. 54

References

COMSOL Multiphysics User's Guide, Release 3.5a. COMSOL, 2008. 3, 37, 63

J. Daněk and H. Kutáková. The mortar finite element method in 2d: implementation in matlab. *16th Annual Conference Proceedings of Technical Computing Prague 2008*, 2008. 54

B.F.M. de Veubeke. *Diffusion des inconnues hyperstatiques dans les voilures à longerons couplés*, volume 24 of *Bulletin du Service Technique de l'Aéronautique*. Imprimerie Marcel Hayez, 1951. 28

A. DeSimone and L. Teresi. Elastic energies for nematic elastomers. *The European Physical Journal E: Soft Matter and Biological Physics*, 29:191–204, 2009. 1

A. DiCarlo and S. Quiligotti. Growth and balance. *Mechanics Research Communication*, 29:449–456, 2002. 5, 11

P.J. Flory. Thermodynamic relations for high elastic materials. *Transactions of the Faraday Society*, 57:829–838, 1961. 18

L.P. Franca and C. Farhat. Bubble functions prompt unusual stabilized finite element methods. *Computer Methods in Applied Mechanics and Engineering*, 123:299–308, 1995. 54

C. Geuzaine and J.-F. Remacle. Gmsh: a three-dimensional finite element mesh generator with built-in pre- and post-processing facilities. *International Journal for Numerical Methods in Engineering*, 79(11):1309–1331, 2009. 37, 63

C. Geuzaine and J.-F. Remacle. *Gmsh Reference Manual.*, October 2010. 3, 37, 63

M.E. Gurtin. *An introduction to continuum mechanics*. Mathematics in science and engineering. Academic Press, 1981. 5, 8

S. Hartmann and P. Neff. Polyconvexity of generalized polynomial-type hyperelastic strain energy functions for near-incompressibility. *International Journal of Solids and Structures*, 40(11):2767–2791, 2006. 2, 19, 53

F. Hecht. *FreeFem++, Version 3.16-1*, 2011. URL `http://www.freefem.org/`. 3

H.C. Hu. Some variational principles in elasticity and plasticity. *Acta Physica Sinica*, 10:259–290, 1954. 28

T. Hughes, J. Cottrell Y., and Bazilevs. Isogeometric analysis: Cad, finite elements, nurbs, exact geometry and mesh refinement. *Computer Methods in Applied Mechanics and Engineering*, 194(39–41):4135–4195, 2005. 54

T.J.R. Hughes. *The Finite Element Method: Linear Static and Dynamic Finite Element Analysis.* Prentice-Hall, Engelwood Cliffs, New Jersey, 1987. 2, 27

H. Jihuan. Equivalent theorem of hellinger-reissner and hu-washizu variational principles. *Journal of Shanghai University (English Edition)*, 1:36–41, 1997. 28

C. Johnson. *Numerical Solution of Partial Differential Equations by the Finite Element Methods.* dover, Mineola New York, 2009. 22, 25, 39

M. Křížek and P. Neittaanmäki. *Finite Element Approximation of Variational Problems and Applications.* Longman Scientific & Technical, Harlow, 1990. 22, 23

P. Nardinocchi and L. Teresi. On the active response of soft living tissues. *Journal of Elasticity*, 88:27–31, 2007. 20, 31

P. Nardinocchi, L. Teresi, and V. Varano. Myocardial contractions and the ventricular pressure–volume relationship. *ArXiv e-prints*, pages 1–16, 2010. 1

W. Noll. La mécanique classique, basée sur un axiome d'objectivité. *La méthode axiomatique dans les méchaniques classiques et nouvelles*, 1963. 12

R.W. Ogden. *Non-Linear Elastic Deformations.* Dover books on physics. Dover Publications, 1997. 13, 14

K.-D. Papoulia. Fully nonlinear hyperelastic analysis of nearly incompressible solids elements and material models in msc nastran. *MSC 1995 World Users' Conference Proceedings*, 1995. 34

P. Podio-Guidugli. *Argomenti Costitutivi in Elasticità. (a series of twelve lectures given at the Scuola Estiva di Fisica Matematica, Ravello, 1993).* published by Scuola Tipo-Litografica "Istituto Anselmi", Marigliano (Napoli), 1994. notes

written with the assistance of P. Nardinocchi and L. Teresi, Quaderni del C.N.R., G.N.F.M. 16

P. Podio-Guidugli. *A Primer in Elasticity.* Kluwer Academic Publishers, Netherlands, 2000. 5, 12, 13, 14, 15

P. Podio-Guidugli. Corso di meccanica dei continui 2009., 2009. Lectures performed at Università degli Studi di Roma "Tor Vergata". 12

E.K. Rodriguez, A. Hoger, and McCulloch. Stress-dependent finite growth in soft elastic tissues. *J. Biomechanics*, 27:455–467, 1994. 11

E. Rohan and R. Cimrman. On macroscopic modelling of smooth muscle. *Pilsen.*, 1999. 1

E. Rohan and R. Cimrman. Sensitivity analysis and material identification for activated smooth muscle. *Comput. Assisted Mechanics Eng. Sci.*, 9(4):519–541, 2002. 1

J. Rosenberg and J. Křen. *Mechanika kontinua.* Skriptum ZČU, Plzeň, 1995. 13

S. Rossi, R. Ruiz-Baier, L.F. Pavarino, and A. Quarteroni. Orthotropic active strain models for the numerical simulation of cardiac biomechanics. *International Journal for Numerical Methods in Biomedical Engineering*, 28(6–7): 761–788, 2012. 20

J.C. Simo and R.L. Taylor. Quasi-incompressible finite elasticity in principal stretches. continuum basis and numerical algorithms. *Comput. Methods Appl. Mech. Eng.*, 85:273–310, February 1991. 27, 53

Barry F. Smith, Petter E. Bjørstad, and William Gropp. *Domain Decomposition: Parallel Multilevel Methods for Elliptic Partial Differential Equations.* Cambridge University Press, 1996. 54

P. Šolín, K. Segeth, and I. Doležel. *Higher-Order Finite Element Methods.* Chapman & Hall / CRC Press, 2003. 54

A. Ženíšek. The finite element method for nonlinear elliptic equations with discontinuous coefficients. *Numerische Mathematik*, 58:51–77, 1990. 2

K. Washizu. *Variational methods in elasticity and plasticity.* International series of monographs on aeronautics and astronautics: Solid and structural mechanics. Pergamon Press, 1974. 28

P. Wriggers. *Nonlinear Finite Element Methods.* Springer-Verlag, Berlin Heidelberg, 2008. 2, 27, 28, 30, 53

O. C. Zienkiewicz, Robert L. Taylor, and J. Z. Zhu. *The finite element method : its basis and fundamentals.* Elsevier Butterworth–Heinemann, 6 edition, 2009. 3, 27

Publications

Articles and chapters in the books

• P. Nardinocchi, T. Svatoň, L. Teresi, *Mechanical response of helically wound fiber-reinforced incompressible non-linearly elastic pipes*, Lecture Notes in Applied and Computational Mechanics, vol. 46, pp. 109–117, 2009.

• P. Nardinocchi, T. Svatoň, L. Teresi, *Torsional deformations in incompressible fibre–reinforced materials*, European Journal of Mechanics – A/Solids, vol. 29, pp. 266–273, 2010.

• A. Carcaterra, O. Giannini, A. Sestieri, T. Svatoň, *The Complex Envelope Vectorization*, "MID-FREQUENCY" – CAE methodologies for Mid-Frequency Analysis in Vibration and Acoustics, 2012.

• A. Carcaterra, O. Giannini, A. Sestieri, T. Svatoň, *Advances in Complex Envelope Vectorization: FEM industrial applications, BEM academic cases and transient dynamics*, Open Journal of Vibration (in preparation), 2012.

Conference proceedings

• P. Nardinocchi, T. Svatoň, L. Teresi, *Using the Comsol in Modeling of Soft Tissues*, 15th Annual Conference Proceedings – Technical Computing Prague, 2007.

• T. Svatoň, P. Nardinocchi, J. Daněk, *Analysis of the Passive Deformation Processes of an Elastic Fibre-Reinforced Tube*, The 1st Young Researchers Conference on Applied Sciences – Conference Proceedings Book, 2007.

• P. Nardinocchi, T. Svatoň, L. Teresi, *Compatible and Mixed Method Application in the Soft Tissue Modelling*, 7th International Conference Aplimat 2008 - Proceedings, 2008.

• T. Svatoň, M. Brandner, J. Daněk, *The Sensitivity of Non-Linear Elliptic Equation Solutions on Boundary Conditions*, 16th Annual Conference Proceedings –

Technical Computing Prague, 2008.

• A. DiCarlo, P. Nardinocchi, T. Svatoň, L. Teresi, *Passive and active deformation processes in cardiac tissue*, Proceedings of the III International Conference on Computational Methods for Coupled Problems in Science and Engineering, 2009.

• A. DiCarlo, P. Nardinocchi, T. Svatoň, L. Teresi, *Passive and Active Deformation Processes of 3D Fibre-Reinforced Caricatures of Cardiovascular Tissues*, Proceedings of the third European COMSOL Conference, 2009.

• A. Carcaterra, A. Sestieri, T. Svatoň, *High-frequency transient vibration: Time-space complex envelope vectorization*, Proceedings of ICEDyn 2011 – International Conference on Structural Engineering Dynamics, 2009.

• A. Carcaterra, A. Sestieri, T. Svatoň, *High-frequency transient vibration: Time-space complex envelope vectorization*, Proceedings of ISCV18 – 18th International Congress on Sound and Vibration, 2011.

• A. Carcaterra, O. Giannini, A. Sestieri, T. Svatoň, *Advances in Complex Envelope Vectorization: industrial applications and transient dynamics*, Proceedings of ISMA2012 (in press), 2012.

Diploma thesis

• T. Svatoň, *A Study of Passive and Active Deformation Processes of a Fibre-Reinforced Cylindrical Dummy of the Beating Heart*, v ZČU, 2007.